Toward a global model of the interactions in low-lying states of methyl cyanide: rotational and rovibrational spectroscopy of the $v_4 = 1$ state and tentative interstellar detection of the $v_4 = v_8 = 1$ state in Sgr B2(N)

Holger S.P. Müller[a,*], Arnaud Belloche[b], Frank Lewen[a], Brian J. Drouin[c], Keeyoon Sung[c], Robin T. Garrod[d], Karl M. Menten[b]

[a] *I. Physikalisches Institut, Universität zu Köln, Zülpicher Str. 77, 50937 Köln, Germany*
[b] *Max-Planck-Institut für Radioastronomie, Auf dem Hügel 69, 53121 Bonn, Germany*
[c] *Jet Propulsion Laboratory, California Institute of Technology, Pasadena, CA 91109-8099, USA*
[d] *Departments of Chemistry and Astronomy, University of Virginia, Charlottesville, VA 22904, USA*

Abstract

Rotational spectra of methyl cyanide were recorded newly and were analyzed together with existing spectra to extend the global model of low-lying vibrational states and their interactions to $v_4 = 1$ at 920 cm^{-1}. The rotational spectra cover large portions of the 36−1439 GHz region and reach quantum numbers J and K of 79 and 16, respectively. Information on the K level structure of CH_3CN is obtained from IR spectra. A spectrum of $2\nu_8$ around 717 cm^{-1}, analyzed in our previous study, covered also the ν_4 band. The assignments in this band cover 880−952 cm^{-1}, attaining quantum numbers J and K of 61 and 13, respectively.

The most important interaction of $v_4 = 1$ appears to be with $v_8 = 3$, $\Delta K = 0$, $\Delta l = +3$, a previously characterized anharmonic resonance. We report new analyses of interactions with $\Delta K = -2$ and $\Delta l = +1$, with $\Delta K = -4$ and $\Delta l = -1$, and with $\Delta K = -6$ and $\Delta l = -3$; these four types of interactions connect all l substates of $v_8 = 3$ in energy to $v_4 = 1$. A known $\Delta K = -2$, $\Delta l = +1$ interaction with $v_7 = 1$ was also analyzed, and investigations of the $\Delta K = +1$, $\Delta l = -2$ and $\Delta K = +3$, $\Delta l = 0$ resonances with $v_8 = 2$ were improved, as were interactions between successive states with $v_8 \leq 3$, mainly through new $v_8 \leq 2$ rotational data.

A preliminary single state analysis of the $v_4 = v_8 = 1$ state was carried out based on rotational transition frequencies and on $\nu_4 + \nu_8 - \nu_8$ hot band data. A considerable fraction of the K levels was reproduced within uncertainties in its entirety or in part, despite obvious widespread perturbations in $v_4 = v_8 = 1$.

In addition to the interstellar detection of rotational transitions of methyl cyanide from within all vibrational states up to $v_4 = 1$, we report the tentative detection of $v_4 = v_8 = 1$ toward the main hot molecular core of the protocluster Sagittarius B2(N) employing the Atacama Large Millimeter/submillimeter Array.

Keywords:
rotational spectroscopy, infrared spectroscopy, vibration-rotation interaction, methyl cyanide, interstellar molecule

1. Introduction

Methyl cyanide was detected in Sagittarius (Sgr) A and B almost 50 years ago as one of the first molecules observed by radio-astronomical means [1]. Since then, the molecule has been found in very diverse astronomical sources, a fairly detailed overview was given in our previous work on vibrational states $v_8 \leq 2$ of CH_3CN [2]. We point out that numerous rare isotopologs have been detected as well, which include $^{13}CH_3{}^{13}CN$ [3] and CHD_2CN [4]. More important for the present study is the detection of excited state transitions of CH_3CN up to $v_4 = 1$ at 920 cm^{-1} [3]; see **Fig. 1** for an overview of the low-lying vibrational states of methyl cyanide and **Table 1** for a summary of the vibrational energies, including those of the l substates.

The identification of gaseous methyl cyanide relies mostly on laboratory spectroscopic information; in astronomical sources

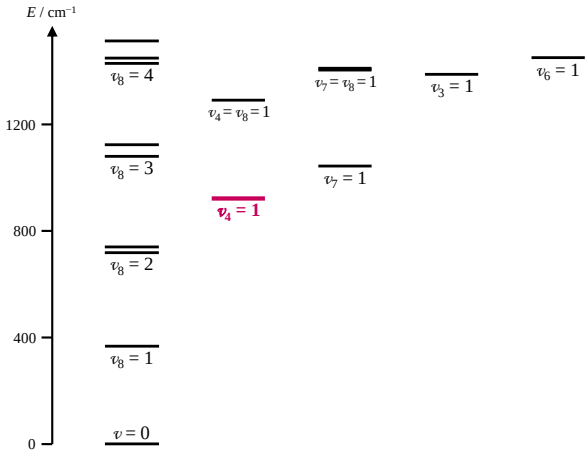

Figure 1: Schematic representation of the energies of low-lying vibrational states of CH_3CN with origins of the l substates.

*Corresponding author.
Email address: hspm@ph1.uni-koeln.de (Holger S.P. Müller)

Table 1: Energies (cm^{-1}) and symmetries Sym of low-lying vibrational states of methyl cyanide.

State	Sym.	Energy	Reference
$v = 0$	A	0.0	per definitionem
$v_8 = 1$	E	365.024	this work, Ref. [2]
$v_8 = 2^0$	A	716.750	this work, Ref. [2]
$v_8 = 2^2$	E	739.148	this work, Ref. [2]
$v_4 = 1$	A	920.290	this work, Ref. [5]
$v_7 = 1$	E	1041.855	Ref. [5]
$v_8 = 3^1$	E	1077.79	this work, Ref. [5]
$v_8 = 3^3$	A	1122.35	this work[a]
$v_4 = v_8 = 1$	E	1290.05	this work
$v_3 = 1$	A	1385.2	Ref. [6]
$v_7 = v_8 = 1^0$	A	1401.7	Ref. [6]
$v_7 = v_8 = 1^2$	E	1408.9	Ref. [6]
$v_8 = 4^0$	A	~1426.	Ref. [2][b]
$v_8 = 4^2$	E	1447.9	Ref. [6]
$v_6 = 1$	E	1449.7	Ref. [6]
$v_8 = 4^4$	E	~1514.	Ref. [2][b]

[a] 1122.15 cm^{-1} in Ref. [5].

[b] Estimated value; see also section 5.

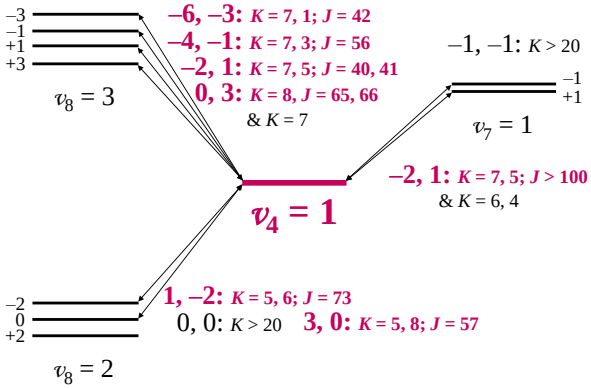

Figure 2: Representation of the rovibrational interactions involving $v_4 = 1$. The l substates of each vibrational state are ordered as they appear at intermediate and higher K. Arrows indicate interacting l substates. ΔK and Δl are given with respect to $v_4 = 1$. The first K refers to $v_4 = 1$, the second to that of the interacting l substate. Distant resonances or resonances with no crossing in J are colored black, resonances with crossing in J in bold and dark red. The most perturbed J is also given.

this is almost exclusively done with rotational spectroscopy from the microwave to the submillimeter region. The first study of the rotational spectrum of CH_3CN, and of its isomer CH_3NC, dates back to the early days of microwave spectroscopy [7]. A detailed account on previous work involving vibrational states up to $v_8 = 2$ was given in our investigation of these states [2]. A Fermi resonance between $v_8 = 1^{-1}$ and 2^{+2} ($\Delta l = 3$) was identified at $K = 13$ and 14 and analyzed by means of rotational spectroscopy. Such resonances occur also between $v_8 = 2^{-2}$ and 3^{+1} at $K = 12$ and 13 and between $v_8 = 2^0$ and 3^{+3} at $K = 15$. Transitions up to $K = 11$ and 13 have been accessed for $v_8 = 2^{-2}$ and 2^0, respectively. This particular type of resonance was reported, to the best of our knowledge, for the first time in studies involving the corresponding bending states of propyne [8, 9, 10]. Rotational spectroscopy was instrumental in untangling analogous resonances. A study of such resonances was also reported for CH_3NC in its $v_8 \leq 2$ states [11]. In the case of CH_3CN, additional resonances of the type $\Delta v_8 = \pm 1$, $\Delta K = \mp 2$, $\Delta l = \pm 1$ were identified and analyzed in detail for $v_8 = 1^{-1}$ and 2^0 ($K = 13$ and 11) and $v_8 = 1^{+1}$ and 2^{+2} ($K = 15$ and 13). Whereas these resonances caused pronounced perturbations, an analogous resonance between $v = 0$ and $v_8 = 1^{+1}$ at $K = 14$ and 12, respectively, displayed only small perturbations. However, these were strong enough to cause observable cross-ladder transitions between the states, thus connecting strongly these two vibrational states in energy.

The analyses of the next three higher-energy states, $v_4 = 1$ at 920 cm^{-1}, $v_7 = 1$ at 1042 cm^{-1}, and $v_8 = 3$ at 1078 and 1122 cm^{-1}, and their interactions took many years until a fairly comprehensive and sufficiently accurate level was achieved. Interactions involving $v_4 = 1$ are shown schematically in **Fig. 2**.

Kondo and Person evaluated the strength of the Coriolis interaction between ν_4 and ν_7 through intensity perturbations of ν_4 in a low-resolution (~1 cm^{-1}) IR spectrum [12]. Bauer [13] studied the rotational spectra of CH_3CN and $CH_3C^{15}N$ up to $v_4 = 1$ (here and in the following, unlabeled atoms refer to ^{12}C and ^{14}N). The $v_4 = 1$ data with $6 \leq J'' \leq 9$ and $K \leq 6$, and with frequencies up to 184 GHz, were published in a journal later [14]. Duncan et al. carried out a comparative study of the IR spectra of several methyl cyanide isotopologs along with a force field calculation [15]. They proposed a strong Fermi interaction between ν_4 and $2\nu_8^0$, a strong anharmonic resonance between ν_4 and $3\nu_8^3$, and a moderate anharmonic resonance between ν_7 and $3\nu_8^1$. Rackley et al. performed a laser Stark investigation of ν_4 and ν_7 and determined in particular a ν_4/ν_7 interaction parameter, even though they point out that the resonance in ν_7^{-1} occurs at $K \approx 23$ [16]. In addition, they examined the $\nu_7^{+1}/3\nu_8^{+1}$ anharmonic resonance, which is most strong at $K = 7$ and 8 [16]. Mori et al. [17] carried out more extensive analyses of CH_3CN IR bands. In addition to the interactions analyzed earlier, they proposed a Fermi resonance between $2\nu_8^{-2}$ and ν_7^{+1} at $K = 13$ and 14. Mito et al. [18] performed a laser Stark investigation of the ν_4 band of $CH_3C^{15}N$ in order to analyze the resonance with $3\nu_8^{+3}$, which they found to be much weaker than proposed by Duncan et al. [15]. They found a crossing between $K = 7$ and 8, with the latter farther apart at low J. Wallraff et al. [19] extended the K range of ν_4 for CH_3CN and obtained essentially the same results concerning the corresponding resonance. Bocquet et al. [20] recorded submillimeter transitions of methyl cyanide, $J'' = 19$ up to $K = 12$ in the case of $v_4 = 1$. Cosleou et al. [21] extended the J range of rotational transitions in $v_4 = 1$ up to 24. They also analyzed the resonance between $v_4 = 1$ and $v_8 = 3^{+3}$, located a $\Delta K = -2$, $\Delta l = +1$ interaction between $v_4 = 1$ and $v_7 = 1^{+1}$ at $K = 6$ and 4, respectively, and proposed a $\Delta K = +3$, $\Delta l = 0$ interaction between $v_4 = 1$ and $v_8 = 2^0$ at $K = 5$ and 8, respectively. The most comprehensive and accurate analysis of the ν_4, ν_7, and $3\nu_8$ band system of CH_3CN was presented by Tolonen et al. [5]. They included most of the resonances mentioned before, with the exceptions of the $\Delta K = 0$ and 3, $\Delta l = 0$ interactions between $v_4 = 1$ and $v_8 = 2^0$. They

introduced a $\Delta K = +1$, $\Delta l = -2$ resonance between $K = 5$ and 6 of $v_4 = 1$ and $v_8 = 2^{-2}$, respectively.

The next five vibrational states are $v_3 = 1$, $v_6 = 1$, $v_4 = v_8 = 1$, $v_7 = v_8 = 1$, and $v_8 = 4$, see **Fig. 1** and **Table 1**. Investigations of the interactions between these states began 50 years ago. Matsuura analyzed the Fermi resonance between $\nu_6^{\pm1}$ and $(\nu_7 + \nu_8)^{\mp2}$ [22]. Duncan et al. [23] and later Matsuura et al. [24] included the Coriolis resonance between ν_6 and ν_3 in their analyses. Paso et al. [6] presented the latest, fairly comprehensive and quite accurate analysis of these bands. Their assignments covered extensive parts of ν_6, a fair fraction of $(\nu_7 + \nu_8)^{\mp2}$, and some transitions in ν_3 ($K = 5$ and 6), which gain intensity through the Coriolis resonance with ν_6. Information on $\nu_4 + \nu_8$, $(\nu_7 + \nu_8)^{\pm0}$, and $4\nu_8^{\pm2}$ were obtained through various resonances; no information was presented for $4\nu_8^0$ and for $4\nu_8^{\pm4}$. A moderately weak anharmonic resonance between $(\nu_4 + \nu_8)^{-1}$ and $(\nu_7 + \nu_8)^{+2}$, mainly at $K = 5$, and a $\Delta K = -1$, $\Delta l = +2$ interaction between $(\nu_4 + \nu_8)^{-1}$ and ν_6^{+1}, mainly at $K = 10$ and 9, respectively, were treated in their analysis. Mito et al. [25] studied the $\nu_4 + \nu_8 - \nu_8$ hot band of $CH_3C^{15}N$ and analyzed an anharmonic resonance between $v_4 = v_8 = 1^{+1}$ and $v_8 = 4^{+4}$ with largest effect at $K = 8$ and a lesser one at $K = 9$ and anharmonic resonances between $v_4 = v_8 = 1^{-1}$, $v_8 = 4^{+2}$, and $v_7 = v_8 = 1^{+1}$ most strongly perturbed at $K = 6$ and less so at $K = 5$. Judging from Fig. 6 of Paso et al. [6], the last three resonances occur at the same K values in CH_3CN, with a possible difference in the resonance between $v_4 = v_8 = 1^{-1}$ and $v_7 = v_8 = 1^{+1}$, which may be strongest in $K = 5$.

Approximately 15 years ago, we started our project devoted to recording and analyzing low-lying vibrational states of methyl cyanide. The aims were providing predictions of rotational and rovibrational spectra for radio-astronomical observations and for studies of the atmospheres of Earth and Titan, among others. An additional, but also necessary aim were thorough investigations of perturbations within and between these vibrational states.

In the course of a line-broadening and -shifting study in the ν_4 band region of CH_3CN [26], a preliminary analysis of $v_4 = 1$ and its interactions with other vibrational states was carried out. In addition, assignments were made for the $\nu_4 + \nu_8 - \nu_8$ hot band and for rotational transitions in $v_4 = v_8 = 1$. Subsequently, extended assignments for the ground state rotational spectra of six methyl cyanide isotopologs were based on measurements on a sample of natural isotopic composition [27]. Some time later, we carried out a similar study of three minor isotopologs, $CH_3{}^{13}CN$, $^{13}CH_3CN$, and $CH_3C^{15}N$, in their $v_8 = 1$ excited vibrational states [28]. The analysis of CH_3CN vibrational states up to $v_4 = 1$ was quite advanced about ten years ago [29]. Attempts to introduce $v_7 = 1$ data into the fit were quite successful, but the inclusion of $v_8 = 3$ data proved to be more difficult. Data for both states were omitted for the present fit because both states are heavily interacting. Ultimately, our previous account on rotational and rovibrational data of CH_3CN [2] was limited to states with $v_8 \leq 2$. The omission of $v_4 = 1$ data at that time was based on large residuals in the $\Delta K = 3$ ground state loops from Ref. [30] and concomitant changes in the purely axial ground state parameters ($A - B$, D_K, H_K). In addition, there were small, but systematic residuals in some K series of the $v_4 = 1$ rotational data.

In our present study, we have reanalyzed carefully our $v_4 = 1$ data, recorded additional rotational transitions pertaining to $v_4 = 1$ and to lower vibrational states as well as to $v_4 = v_8 = 1$. We improved the analyses of all known resonances involving $v_4 = 1$ and those involving states differing in one quantum of v_8. Three higher-ΔK resonances between $v_4 = 1$ and $v_8 = 3$ were also investigated. These findings improve the parameters for $v_4 = 1$ considerably and for some of the lower states to a lesser extent. We also report a preliminary analysis of $v_4 = v_8 = 1$. We use the spectroscopic results obtained for $v_4 = 1$ and $v_4 = v_8 = 1$ in this study to investigate the vibrationally excited methyl cyanide emission in the main hot molecular core embedded in the high-mass star forming protocluster Sagittarius B2(N) observed with the Atacama Large Millimeter/submillimeter Array (ALMA) in the frame of the ReMoCA project [31].

The remainder of this article is outlined as follows: experimental details of the rotational and rovibrational spectra are given in Section 2; Section 3 contains our results with details on the spectroscopy and interactions in low-lying vibrational states of CH_3CN, descriptions of the analyses carried out in the present study, a summary of the data obtained newly as well as those from previous investigations, and the determination of spectroscopic parameters. The astronomical results are described in Section 4; a discussion of the spectroscopic findings is presented in Section 5; Section 6 finally presents conclusions and an outlook from our study.

2. Experimental details

2.1. Rotational spectra at the Universität zu Köln

All measurements at the Universität zu Köln were recorded at room temperature in static mode employing different Pyrex glass cells having an inner diameter of 100 mm with pressures in the range of 0.5−1.0 Pa below 368 GHz, around 1.0 Pa between 1130 and 1439 GHz, and mostly 2 Pa up to 4 Pa between 748 and 1086 GHz. The measurements covered transitions pertaining to one J of one or more vibrations in many cases, sometimes smaller groups of lines, and in many cases individual lines. The window material was Teflon at lower frequencies, whereas high-density polyethylene was used at higher frequencies. Frequency modulation was used throughout. The demodulation at $2f$ causes an isolated line to appear close to a second derivative of a Gaussian.

The $J = 4 - 3$ transitions of $v_4 = 1$ near 73 GHz were recorded using a 3 m long single pass cell, a backward-wave oscillator (BWO) based 4 mm synthesizer AMC MSP1 (Analytik & Meßtechnik GmbH, Chemnitz, Germany) as source, and a Schottky-diode as detector. A small number of methyl cyanide rotational transitions were investigated around 875 GHz and around 892 GHz with the Cologne Terahertz Spectrometer [32] using a BWO as source and a liquid helium cooled InSb hot-electron bolometer (QMC) as detector.

Transitions of $J = 2 - 1$ and $3 - 2$ around 37 and 55 GHz, respectively, were recorded with an Agilent E8257D microwave

synthesizer as source and a home-built Schottky diode detector. A 7 m long double pass absorption cell was used for these measurements. Transitions of $J = 4 - 3$ to $6 - 5$ were measured in two coupled 7 m long double pass absorption cells. Source frequencies were generated using a Virginia Diodes, Inc. (VDI) tripler driven initially by an Agilent E8257D microwave synthesizer, later by a Rohde & Schwarz SMF 100A synthesizer, and a Schottky diode detector was employed again. Additional information on the spectrometer is available elsewhere [33].

Further transitions were covered in the 164−368 GHz region employing a 5 m long double pass absorption cell, VDI frequency multipliers driven by a Rohde & Schwarz SMF 100A synthesizer, and Schottky diode detectors. Ref. [34] contains more information on this spectrometer. Uncertainties down to 3 kHz were assigned for very symmetric lines with very good signal-to-noise ratio recorded with these two frequency multiplier based spectrometers. Almost as small uncertainties ($\geq$ 5 kHz) were assigned in a study of 2-cyanobutane [35], which has a much richer rotational spectrum. Lines of average quality were assigned 10−20 kHz uncertainties, up to 50 kHz for weaker lines or lines close to stronger ones.

Measurements were also carried out in parts of the 1130−1439 GHz region employing a 3 m long single pass cell, two VDI frequency multipliers driven by an Agilent E8257D microwave synthesizer as source, and a liquid He-cooled InSb bolometer (QMC) as detector. This spectrometer was described in somewhat greater detail in the investigation of CH_3SH [36]. Our latest CH_3CN study [2] or an investigation of isotopic thioformaldehyde [37] demonstrate that accuracies of 10 kHz can be reached readily routinely for very symmetric lines with good signal-to-noise ratios (S/N). Lines of average quality have uncertainties of 30 to 80 kHz, weaker lines, less symmetric lines or close to stronger lines were assigned uncertainties of 100 to 200 kHz, sometimes up to 300 kHz.

A similar setup with a 5 m long single pass cell, a VDI frequency multiplier driven by a Rohde & Schwarz SMF 100A microwave synthesizer as source, and a closed cycle liquid He-cooled InSb bolometer (QMC) as detector was used to cover transitions in the 748−1086 GHz region.

2.2. Rotational spectra at the Jet Propulsion Laboratory

The CH_3CN rotational spectra taken with the JPL cascaded multiplier spectrometer [38] are the same as employed for our latest two studies [2, 28]. Generally, the output of a multiplier chain source is passed through a 1−2 meter pathlength flow cell and is detected by a silicon bolometer cooled to near 1.7 K. The cell is filled with a steady flow of reagent grade acetonitrile at room temperature, and the pressure and modulation are optimized to enable good S/N with narrow lineshapes. The S/N ratio was optimized for a higher-K transition (e.g. $K = 12$) because of the very strong ground state transitions of the main isotopolog with lower K, which frequently exhibit saturated line profiles. This procedure enables better dynamic ranges for the extraction of line positions for rare isotopologs and highly excited vibrational satellites. The frequency ranges covered were 440−540, 530−595, 619−631, 638−648, 770−855, 780−835, 875−930, 967−1050, 1083−1093, 1100−1159, 1168−1198, 1576−1591, and 1614−1627 GHz. Most of the employed multiplier sources were previously described [2, 38]. In addition, recording conditions and sensitivities of detectors can have strong influences on the quality of the spectra. Particularly good S/N were reached around 600, 800, 900 and at 1100−1200 GHz. The S/N changed considerably within each scan and was usually lower towards the edges. The uncertainties were judged exactly as the submillimter lines measured in Cologne, however, the distribution of the uncertainties differed somewhat with fewer lines having very small uncertainties and more lines in the 50−100 kHz range.

2.3. Infrared spectrum

The lower wavenumber part of the infrared spectrum of CH_3CN, recorded between 600 and 989 cm^{-1}, was already used in our previous study [2]. It was recorded at the Pacific Northwest National Laboratory (PNNL) with a Bruker 125 HR Fourier transform spectrometer at 0.0016 cm^{-1} resolution using an MCT detector. A multi-pass absorption cell, set to an optical path length of 19.20 m, was filled to 0.226 Torr (30.1 Pa) of CH_3CN at 293.0 K. Small amounts of OCS (~3%) and CO_2 (~0.4%) were added to the sample for frequency calibration. Comparison of 63 well-isolated lines of the ν_3 fundamental of OCS at 860 cm^{-1} [39] produced a calibration factor 1.000000868 (21) with an rms of 0.0000182 cm^{-1}. Nearly 9000 line positions and relative intensities between 880 and 952 cm^{-1} were retrieved using non-linear least-squares curve-fitting [40]. The accuracy in ν_4 was 0.0001 cm^{-1}, about a factor five worse than the OCS calibration because of the congestion of the CH_3CN spectrum. Uncertainties in $\nu_4 + \nu_8 - \nu_8$ were mostly 0.0002 or 0.0004 cm^{-1} because of the greater congestion compared with ν_4.

3. Results

Pickett's SPCAT and SPFIT programs [41] were used for calculations of the CH_3CN spectra and for fitting of the measured data. The programs were intended to be rather general, thus being able to fit asymmetric top rotors with spin and vibration-rotation interaction. They have evolved considerably with time because many features were not available initially [42, 43], in particular special considerations for symmetric or linear molecules or for higher symmetry cases. One of the latest additions is the option to define l-doubled states having $l \equiv 0 \bmod 3$.

We determined rotational, centrifugal, and hyperfine structure (HFS) parameters of the ground state as common for all vibrational states. Some of the data were measured or reported with partial or fully resolved HFS, but the majority of the data, in particular the IR data, were not affected by HFS. Therefore, all states were defined twice, with and without HFS. Vibrational changes $\Delta X = X_i - X_0$ to the ground vibrational state were fit for excited vibrational states, where X represents a parameter and X_i and X_0 the parameter in an excited and ground vibrational state, respectively. This is very similar to several previous studies on CH_3CN, for example [5, 6] and rather convenient because

vibrational corrections ΔX are usually small with respect to X, especially for lower order parameters X. Moreover, this offers the opportunity to constrain vibrational corrections to $v_8 = 2$ to twice those of $v_8 = 1$ wherever appropriate, thus reducing the amount of independent spectroscopic parameters further. New parameters in the fit were chosen carefully by searching for the parameter that reduces the rms error of the fit the most. We tried to assess if the value of a new parameter is reasonable in the context of related parameters and tried to omit or constrain parameters whose values changed considerably in a fit or had relatively large uncertainties. Care was also taken that a new parameter is reasonable with respect to quantum numbers of newly added transition frequencies or that it can account for systematic residuals.

The spectroscopic parameters used in the present analyses are standard symmetric rotor parameters defined and designated in a systematic way. The designation of the interaction parameters in particular may differ considerably with respect to other publications, and there may be small changes in the details of their definitions. Therefore, we give a summary of the interaction parameters in the following. Fermi and other anharmonic interaction parameters are designated with a plain F and are used in the same way irrespective of a $\Delta l = 0$ or $\Delta l = 3$ interaction because the SPFIT and SPCAT programs use only $l = 0$ and ± 1. The parameters G_b and F_{ac} are first and second order Coriolis-type parameters, respectively, of b-symmetry, i.e., they are coefficients of iJ_b and $(J_aJ_c + J_cJ_a)/2$, respectively. The parameters G_a and F_{bc} are defined equivalently. The interacting states are given in parentheses separarated by a comma; the degree of excitation of a fundamental and the l quantum number are given as superscripts separated by a comma if necessary. Rotational corrections to these three types of parameters are designated with J and K subscripts, respectively, as is usually the case. There may also be $\Delta K = \Delta l = 2$ corrections (i.e. $J_+^2 + J_-^2$; where $J_\pm = J_a \pm iJ_b$) to these parameters; they are indicated by a subscript 2. Higher order corrections with $\Delta K = \Delta l = 4$ etc. are defined and indicated equivalently. Additional aspects relevant to the spectroscopy of CH_3CN were detailed earlier [2]. Further, and more general information on SPFIT and SPCAT is available in Refs. [44] and [45] and in the Fitting Spectra section[1] of the Cologne Database for Molecular Spectroscopy, CDMS [46, 47].

After a brief description of the spectroscopy of CH_3CN and interactions in low-lying vibrational states, we summarize the previous data situation for individual states, the new data, and important aspects of the added spectroscopic parameters, starting with $v_4 = 1$ because it is the most extensive addition to our global fit of low-lying CH_3CN vibrational states. After presentation of the global fit parameters, we summarize our findings for $v_4 = v_8 = 1$.

3.1. Overview of the spectroscopy and interactions in low-lying vibrational states of CH_3CN

The six atoms in methyl cyanide lead to 12 vibrational degrees of freedom, four totally symmetric and four doubly degenerate fundamentals. The three lowest energy fundamentals are the doubly degenerate CCN bending mode ν_8 at 365.024 cm^{-1} [2], the totally symmetric CC stretching mode ν_4 at 920.290 cm^{-1} [5], and the doubly degenerate CH_3 rocking mode ν_7 at 1041.855 cm^{-1} [5]. These bands are comparatively weak with integrated room temperature cross sections in the range 2 to 5×10^{-19} cm/molecule.

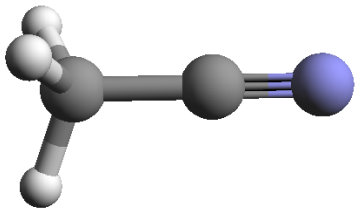

Figure 3: Model of the methyl cyanide molecule. The C atoms are shown in gray, the H atoms in light gray, and the N atom is shown in blue. The a-axis is along the CCN atoms and is also the symmetry axis.

Methyl cyanide is a strongly prolate molecule ($A \gg B$) because the light H atoms are the only ones not on the symmetry axis of CH_3CN, as indicated in **Fig. 3**. Rotational transitions obey the $\Delta K = 0$ selection rules. The large dipole moment of 3.92197 (13) D [48] causes the transitions to be particularly strong. $\Delta K = 3$ transitions only gain intensity through centrifugal distortion effects and are usually too weak to be observed. The purely axial parameters A (or $A - B$), D_K, etc. cannot be determined by rotational spectroscopy, unless perturbations are present. Rovibrational spectroscopy yields, strictly speaking, the differences ΔA (or $\Delta(A - B)$), ΔD_K, etc. from single state analyses. Thus, the ground state axial parameters cannot be determined from such fits either. In the case of CH_3CN, they were determined through analyses of three IR bands involving two doubly degenerate vibrational modes, ν_8, $\nu_7+\nu_8$, and $\nu_7+\nu_8-\nu_8$ [30] and improved through perturbations [2].

The value of A, ~5.27 cm^{-1}, leads to a rapid increase in rotational energy with K. The $J = K = 9$ level is at 429 cm^{-1}, higher than the vibrational energy of $v_8 = 1$. The highest K levels observed involve $K = 21$, and the $J = K = 21$ energy is at 2313 cm^{-1}.

Low-lying degenerate bending modes commonly display strong Coriolis interaction between the l components. The Coriolis parameter ζ in $v_8 = 1$ of CH_3CN is 0.8775, close to the limiting case of 1. The K levels with $l = +1$ are pushed down in energy, and those with $l = -1$ are pushed up with the result that levels differing in K by ± 2 and in l by ± 2 are close in energy. These levels have the same symmetry and can thus repel each other through the q_{22} interaction, which causes widespread effects in $v_8 = 1$ and its overtone states. The $v = 0$ K levels rise in energy faster than those of $v_8 = 1^{+1}$ because of the shift of those K levels to lower energies, see for example Fig. 4 in Ref. [2]. The $K = 14$ levels of $v = 0$ and those of $K = 12$ of $v_8 = 1^{+1}$ cross between $J = 42$ and 43. The effects are small ($\leq$ 25 MHz) and rather localized to ~12 transitions in each vibrational state, of which several shifts are below 1 MHz. Nevertheless, the observation of the most perturbed transitions

[1] See https://cdms.astro.uni-koeln.de/classic/pickett

within each state and the much weaker transitions between the vibrational states introduced a very accurate local constraint on the CH_3CN energy level structure.

There are three l components in the case of $v_8 = 2$, $l = 0$ with $E_{vib} = 716.750\ cm^{-1}$ and $l = \pm 2$ with $E_{vib} = 739.148\ cm^{-1}$ [2]. The effective strength of the Coriolis interaction between the $l = +2$ and $l = -2$ levels is two times that betwen the l components in $v_8 = 1$, causing not only levels with $\Delta K = \pm 2$ and $\Delta l = \pm 2$ to be close in energy, but also those with $\Delta K = \pm 4$ and $\Delta l = \pm 4$. There is a q_{22} resonance between $K = 2$ of $v_8 = 2^{-2}$ and $K = 4$ of $v_8 = 2^0$. Consequently, transitions of the nominally forbidden $2\nu_8^{\pm 2}$ band gain substantial intensity and are almost as strong as $2\nu_8^0$ for levels close to the resonance. This facilitated an accurate determination of the origin of $2\nu_8^{\pm 2}$. The shifts in the K levels in $v_8 = 1$ and 2 produce a level crossing between $K = 13$ and 14 for $v_8 = 1^{-1}$ and $v_8 = 2^{+2}$, a Fermi resonance with $\Delta l = 3$. Large effects of resonances such as this are fairly localized in K, but usually widespread in J.

Interactions with $\Delta v_8 = \pm 1$, $\Delta K = \mp 2$, $\Delta l = \pm 1$, such as that between $v_8 = 0$ and 1, occur also between $v_8 = 1$ and 2 and have been analyzed in our previous study [2], as have been $\Delta l = 3$ Fermi resonances between $v_8 = 2$ and 3 through rotational transitions in $v_8 = 2$. Additional information will be given in Section 3.3.1.

Adding the K levels of $v_4 = 1$ and $v_7 = 1$ between $v_8 = 2$ and 3 to the picture creates many more opportunities for resonant or near-resonant interactions as mentioned in the introduction and to some extent in the following section. Moving up in energy increases the number of vibrational states and potential resonances rapidly.

3.2. The $v_4 = 1$ state

Around 2014, when our fit of low-lying vibrational states of CH_3CN was restricted to $v_8 \leq 2$, the $v_4 = 1$ data set contained more than two thirds of the final ν_4 lines; mostly lines with high J or K and Q-branch lines were added later. The rotational data at that time consisted of earlier published data with $J'' = 6$ to 9 [14], $J'' = 19$ [20], and $J'' = 18$, 20, and 23 [21], of which the $J'' = 6$, 7, and 23 lines were retained in the final line list. Transitions with $J'' = 24$ to 64 between 455 GHz and almost 1.2 THz were extracted from the spectra taken at JPL; transitions with $J'' = 86$ at almost 1.6 THz were too noisy and were omitted from the final line list. Spectra in the fit taken in Cologne covered at that time $J'' = 3$, high-K lines of $J'' = 47$ and 48 and several transitions with $J'' = 61$ to 78 at 1.11 to 1.44 THz to varying degrees. The lines were straightforward to assign, except few very perturbed lines.

Fitting the lines was much more challenging, as a large number of distortion parameters appeared to be needed and some, mostly small, but systematic residuals remained. Moreover, all attempts fitting the $v_4 = 1$ data led to large residuals in the ground state $\Delta K = 3$ loops and changes in the purely axial ground state parameters well outside the uncertainties. In order to see the effect and the quality of newly added $v_4 = 1$ data or the influence of added parameters on the fit more easily, we performed a refit of $v_4 = 1$ initially constrained to only the rotational data in this state. In order to account for the effects

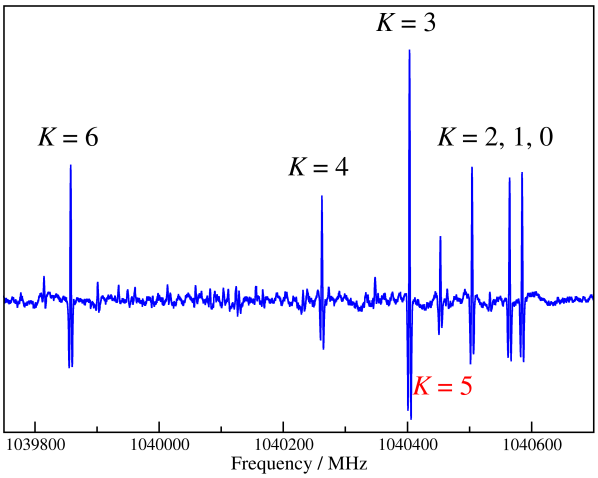

Figure 4: Section of the $v_4 = 1$ rotational spectrum of CH_3CN displaying part of the $J = 57 - 56$ transitions. The $K = 5$ transition has been shifted higher in frequency because of the resonance with $K = 8$ of $v_8 = 2^0$.

caused by interactions with other vibrational states, we took the entire spectroscopic parameter set from our previous study [2] and kept all parameters fixed. Parameters were floated or new parameters added only if this resulted in a substantial improvement of the rms error as a measure of the quality of the fit. At each step, care was taken to float or add only the parameter that resulted in the greatest improvement of the rms error.

3.2.1. Rotational data and analysis

The refit was started with initial rotational data up to 440 GHz which encompassed the previously published data [14, 20, 21] and the $J'' = 3$ lines from Cologne. Most of the transition frequencies were calculated quite well by the initial parameters with the exception of the $K = 12$ lines, which were reported almost 1 MHz lower. The rms error before the fit of almost 2.0 was reduced to slightly below 1.0 with small to modest changes in the $v_4 = 1$ parameters.

Addition of $J'' = 1$, 2, 4, and 5 data caused minor changes. Many of these and of the $J'' = 3$ transitions displayed partially or fully resolved ^{14}N hyperfine splitting. In addition, we observed some of the weaker $\Delta F = 0$ components. These data established that the excitation of v_4 affects the hyperfine structure negligibly as we obtained $\Delta eQq = -1.0 \pm 4.1$ kHz. This parameter was tested later again with essentially the same result and therefore not retained in the final fit.

The subsequent increase in J, $J'' = 24$ to 27 were added next to the line list, but more importantly the increase in K to 15 required octic distortion parameters to be included, in particular ΔL_{KKJ} together with ΔL_{JK}. Addition of $J'' = 28$ to 34 up to 640 GHz did not yet require further parameters, but perturbations in the $K = 7$ lines could not be accounted by the initial interaction parameters. However, the effects were small, less than 0.36 MHz, and the lines were given reduced weights preliminarily, effectively ignoring the perturbation at this stage of the analysis.

The addition of series of transitions with higher J (≥ 42) did not yield satisfactory results with one or two additional $v_4 = 1$ distortion parameters. This situation did not change by adding newly recorded transitions in the 2 and 1 mm regions with $8 \leq J'' \leq 19$ and K up to 16.

In order to test if the difficulties fitting the higher-J $v_4 = 1$ data were caused by interactions with other vibrational states, we combined the $v_4 = 1$ rotational data up to $J'' = 34$ with the ν_4 assignments existing at that time and the $v_8 \leq 2$ data from Ref. [2] supplemented by data recorded at 2 and 1 mm in the course of the present investigation as detailed in Sections 3.3.1 and 3.4.1. The spectroscopic parameters were essentially those of the previous study, with the exception for $v_4 = 1$, for which we took the latest set of parameters. The change in parameter values was small in most cases, and often within the present uncertainties. Notable exceptions were $\Delta(A - B)$, ΔD_K, and ΔH_K, which took values quite close to the now final ones, as well as $F_{ac}(8^{2,\pm2}, 4^1)$ and $F_{2ac}(8^{2,0}, 4^1)$, which describe the interactions between $v_8 = 2$ and $v_4 = 1$. Even though the ground state purely axial parameters changed little, they were kept fixed in the fit for now.

The addition of $K = 0$ to 3 lines with $J'' \leq 79$ caused a pronounced change in ΔD_J and a relatively larger one in ΔH_J. The parameter ΔL_{JJK} was added to the fit later. In the course of fitting these data, additional, limited measurements in the 748−1077 GHz region were made for $K = 3$, 4, and 10 to 15, and more extensive measurements were made for $K = 5$ to 9 in order to improve the analyses of the interactions between $v_4 = 1$ with other vibrational states. The impact of including $K = 4$ lines up to high J in the fit was small. Subsequently, lines with $K = 5$, 6, 7, 9, and 8 were added one after the other.

There is a crossing in energy between $K = 5$ and 6 of $v_4 = 1$ and $K = 6$ and 7 of $v_8 = 2^{-2}$ on one hand and $K = 8$ and 9 of $v_8 = 2^0$ on the other hand, see **Fig. 2** and also the K-level diagram in Fig. 2 of Ref. [5]. Resonances occur in $K = 5$ of $v_4 = 1$ at $J = 73$ in the first case and at $J = 57$ and $K = 8$ in the second case. The previous line list contained the $J'' = 74$ transition of $v_8 = 2^{-2}$, $K = 6$ in the vicinity of the first resonance. We added $J'' = 71$ and 75−77 of $v_4 = 1$, $K = 5$ in the present study and, at the resonance, the two slightly stronger $J = 73 - 72$ transitions between the states and the weaker transition within $v_4 = 1$. In the case of the second resonance involving $K = 8$ of $v_8 = 2^0$ ($\Delta K = 3$), our previous line list already contained $J'' = 55$ and 56. In the course of the present investigation, we recorded the $J'' = 57$ and 58 transitions as well as the weaker $J = 57 - 56$ and $58 - 57$ transitions between both vibrational states. The displacement of the $J = 57 - 56$, $K = 5$ transition is shown in **Fig. 4**. The transitions associated with these resonances in $K = 5$ of $v_4 = 1$ affected not only the value of $F_{2ac}(8^{2,0}, 4^1)$, but also the $v_8 = 2^{\pm2}$ parameters; for example, η_K of $v_8 = 2^{\pm2}$ was now essentially equal to η_K of $v_8 = 1$ and ΔD_K of $v_8 = 2^{\pm2}$ was nearly identical to ΔD_K of $v_8 = 2^0$, as one would expect.

A crossing in energy occurs also between $K = 6$ and 7 of $v_4 = 1$ and $K = 4$ and 5 of $v_7 = 1^{+1}$. The energy difference at $J = 6$ of $K = 6$ and 4 is 6.2 cm^{-1}, increasing to 14.3 cm^{-1} at $J = 78$, the highest value in our line list. In contrast, the energy

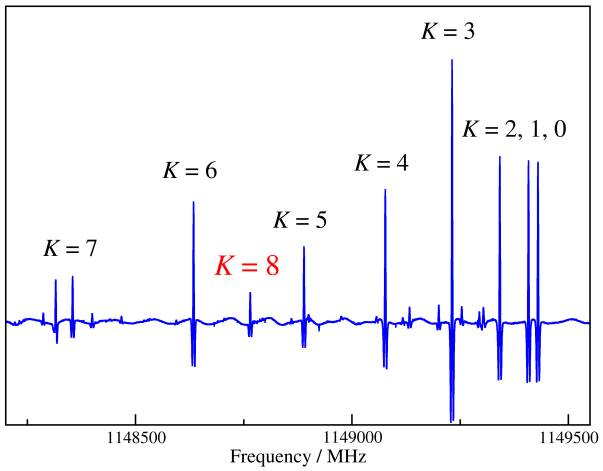

Figure 5: Section of the $v_4 = 1$ rotational spectrum of CH_3CN displaying part of the $J = 63 - 62$ transitions. The $K = 8$ transition has been shifted higher in frequency because of the resonance with $K = 8$ of $v_8 = 3^{+3}$. The largest perturbation occurs for $J = 66 - 65$, see also **Fig. 6**.

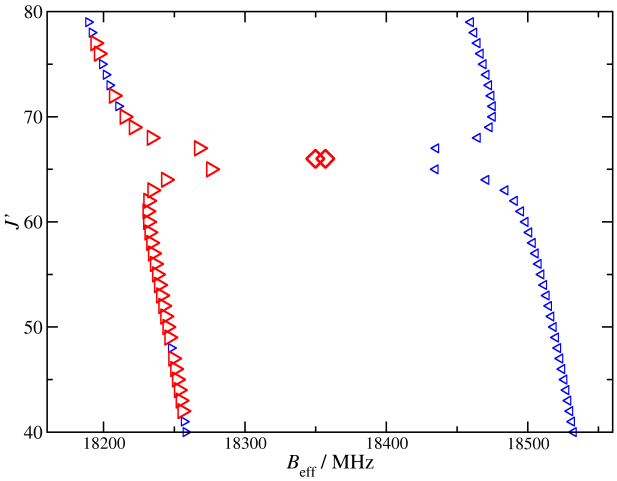

Figure 6: Section of the Fortrat diagram of the rotational spectrum of CH_3CN displaying the anharmonic resonance between $K = 8$ of $v_4 = 1$ (left) and $v_8 = 3^{+3}$ (right). Measured transitions in the final fit are shown in large triangles (online red), calculated transitions in smaller ones (online blue). The two transitions at $J' = 66$ are nominally between the states and shown as diamonds; see also **Fig. 5**.

difference at $J = 7$ of $K = 7$ and 5 is 18.7 cm^{-1}, decreasing to 9.4 cm^{-1} at $J = 78$. Even though a crossing is predicted to occur at J well above 100, it appears as if the perturbation in $K = 6$ of $v_4 = 1$ contributes more to the interaction parameter than the perturbation in $K = 7$.

Particularly challenging was fitting the $K = 7$ and 8 transitions. First, there is a crossing between $K = 7$ and 8 of $v_4 = 1$ with $K = 7$ and 8 of $v_8 = 3^{+3}$. At low J, the effect is larger in $K = 7$, as the energy difference is 8.0 cm^{-1}, while it is 19.6 cm^{-1} in $K = 8$. But the energy difference in $K = 7$ increases to 35.7 cm^{-1} at $J = 78$, the highest value in our present data set, whereas there is a resonance at $J = 65$ and 66 in $K = 8$. The perturbations are pronounced already a few J below the resonance, as can be seen in **Fig. 5**. The Fortrat diagram in **Fig. 6** demonstrates the good coverage of transitions in the fit on the $v_4 = 1$ side which include in particular the most strongly perturbed $J = 66 - 65$ transitions nominally between the two vibrational states. There are, however, additional resonances in $K = 7$ of $v_4 = 1$, first with $K = 5$ of $v_8 = 3^{+1}$ at $J = 40$ and 41, second with $K = 3$ of $v_8 = 3^{-1}$ at $J = 56$, and finally with $K = 1$ of $v_8 = 3^{-3}$ at $J = 42$. In other words, $v_8 = 3$ is linked with all of its l-components to $v_4 = 1$ through rovibrational interactions.

The addition of high-J lines with $K = 7$ improved $F(4, 8^{3,\pm3})$ considerably and $F_2(4, 8^{3,\pm1})$ even more so. The parameters ΔP_{KJ} and ΔP_{JK} were added to the fit with the $K = 9$ lines.

The inclusion of high-J lines with $K = 8$ required in particular the adjustment of some $v_8 = 3^{\pm3}$ parameters. The origin was floated first, followed by ΔB. Floating $A\zeta$ also improved the fit, but the minimum was much flatter than suggested by its uncertainty. The value of 138720 MHz was quite different from the initial 138527.8 MHz, but fairly close to 138656.0 and 138655.3 MHz determined in our present fits for $A\zeta$ of $v_8 = 1$ and 2, respectively. We estimated for $v_8 = 3^{\pm3}$ a value of 138654.8 MHz and kept this value fixed. Subsequently, we also floated the origin of $v_8 = 3^{\pm1}$. Additional $v_4 = 1/v_8 = 3$ interaction parameters included in late fits are $F_J(4, 8^{3,\pm3})$, $F_{2J}(4, 8^{3,\pm1})$, $F_4(4, 8^{3,\mp1})$, and $F_6(4, 8^{3,\mp3})$ with which almost all of the $K = 7$ transitions of $v_4 = 1$ were calculated well. They cover for example $J'' = 43$ to 62 with the exception of $J'' = 50$ and 59. Unfortunately, it was difficult to fit either of the two potential $J = 43 - 42$ transition frequencies at 785142.02 and 785181.83 MHz. The former line matches better the expected intensity whereas the latter is slightly closer to the presently calculated frequency of 785163.61 MHz. The line list contains three potential $J = 42 - 41$ transition frequencies; two also ∼20 MHz to either side of the present calculation and one with more than 50 MHz possibly too far away. The late observation of the $J = 41 - 40$ transition was instrumental for solving the puzzle. One line of correct intensity for this transition was found only ∼5 MHz higher than from a very late calculation. This line was easily accomodated by the fit. The value of F_2 was changed slightly, its uncertainty improved considerably. In contrast, the values of F_4 and F_6 changed relatively more, and their uncertainties were less improved. The calculated transition frequencies of $J'' = 41$ and 42 changed only by slightly more than 1 MHz. The over- or underestimation of the strength of the $\Delta K = -6$, $\Delta l = -3$ resonance between $v_4 = 1$ and $v_8 = 3$ most likely explains the presently poor fitting of the $K = 7$, $J'' = 41$ and 42 transitions. The authors of Ref. [5] define ΔX with opposite sign than we do. Their experimentally determined ΔA of $v_8 = 3^3$ is 266 MHz, whereas their extrapolated value is 376 MHz, a difference of 110 MHz. This large discrepancy prompted us to try to increase our $\Delta(A-B)$ in magnitude in order to fit these two transitions better. A value of −392.7 MHz reproduced the $J'' = 42$ candidate line with the correct intensity and one of the $J'' = 41$ lines within uncertainties. Two ν_4 transitions with $K = 7$ and $J' = 42$ and with the correct intensities, however, were observed ∼40 MHz lower than calculated, suggesting two other candidate transitions to be the correct ones. In contrast to expectations, $\Delta(A - B)$ had to be enlarged even further in magnitude to −442.06 MHz, almost to the extrapolated value [5]. Noting that several other $v_8 = 3$ parameters differ from what we would extrapolate from our $v_8 = 1$ and 2 parameters, we adjusted ΔD_K of $v_8 = 3$ and $A\zeta$ of $v_8 = 3^1$ in order to test the effects on $\Delta(A - B)$ of $v_8 = 3^3$. The resulting changes on $\Delta(A - B)$ of $v_8 = 3^3$ were ∼0.5 MHz in magnitude, but canceled due to their opposite signs. Changes to all other spectroscopic parameters were very small and affected the weighted rms of the fit very little, such that we refrained from adjusting further $v_8 = 3$ parameters. Inspection of the energy levels of $J = 42$ revealed that $K = 1$ of $v_8 = 3^{-3}$ has changed from 3335 MHz or 0.11 cm^{-1} below $K = 7$ of $v_4 = 1$ before the fit to 1979 MHz or 0.066 cm^{-1} above $K = 7$ of $v_4 = 1$ after the fit. It is thus the perturbation between these levels which accounts for the initial deviations and for the subsequent constraining of $\Delta(A - B)$ of $v_8 = 3^3$. In this context it is remarkable that the $\Delta K = 6$ term $F_6(4, 8^{3,\mp3})$ could be omitted from the final fit. The proximity of $K = 5$ of $v_8 = 3^{+1}$ to $K = 1$ of $v_8 = 3^{-3}$, less than **0.6** cm^{-1} for J up to 45, may affect these results somewhat in later analyses with extensive $v_8 = 3$ data.

Adding the high-J lines ($J'' \leq 64$) with $K = 10$ and 11 did not change parameter values much. Adding those with $K = 12$ to 15, the last one up to $J'' = 60$ and the remaining high-K transitions with low values of J afforded ΔP_{KKJ} in the fit.

Trial fits with $G_b(4, 7)$ increased changed the $v_4 = 1$ distortion parameters little and did not improve the quality of the fit. This also applied to trial fits with various values of $F(4, 8^{2,0})$ in order to test the effect of a purported strong Fermi resonance between $v_8 = 2^0$ and $v_4 = 1$ [15].

3.2.2. The ν_4 band

No line lists were provided with the earlier combined analysis of ν_4, ν_7, and $3\nu_8$ [5]. Therefore, we relied entirely on our new spectrum which is shown in **Fig. 7**. A pronounced Herman-Wallis effect causes the P-branch to be substantially stronger than the R-branch. Assignments in P- and R-branches of the ν_4 cold band were straightforward based on the earlier analysis. Nevertheless, ground state combination differences were used in the initial round to establish the assignments. The assignments were extended to J of 56 and 61 in the P- and R-branches, respectively, and up to $K = 13$ in the final rounds, taking relative intensities strongly into account. While many transitions with $K = 12$ had good or very good S/N, almost all of the $K = 13$ lines were near or below the detection limit.

Table 2: Maximum J value and K values and number of rotational and IR lines in vibrational substates of methyl cyanide used in the present / previous study[a], with numbers retained in the present fit from previous data in parentheses and rms error for subsets of data.

	$v = 0$	$v_8 = 1^{+1}$	$v_8 = 1^{-1}$	$v_8 = 2^{0}$	$v_8 = 2^{+2}$	$v_8 = 2^{-2}$	$v_4 = 1$
J_{max}(rot)	89/89	88/88	88/88	88/88	88/88	88/88	79/24
K_{max}(rot)	21/21	20/20[b]	17/17	13/13[c]	19/19[c]	11/11	16/12
no. of rot lines[d]	316/316	605/596	549/527	488/424	607/546	351/299	705/86
rms[e] / kHz	21.9/22.2	43.3/43.7	40.6/39.9	52.6/60.9	54.5/58.1	53.9/78.2	51.2/–
rms error[e]	0.862/0.859	0.803/0.807	0.797/0.796	0.965/0.982	0.906/0.915	0.971/0.957	1.021/–
J_{max}(IR)	–/–[f]	71/71	74/74	67/66	57/53	66/66	61/73
K_{max}(IR)	7/7	11/11	11/11	13/12	2/2	5/7	13/12
no. of IR lines[d]	5/5[f]	836/836	861/861	963/935	57/40	195/197	1290/1173
rms / 10^{-4} cm^{-1}	0.07/0.04	0.22/0.22	0.19/0.19	0.17/0.19	0.26/0.38	0.20/0.24	0.09/0.13
rms error[e]	1.328/0.716	0.847/0.826	0.797/0.797	0.634/0.771	0.836/849	0.703/0.727	0.920/–

[a] Previous data from Ref. [2] and references therein for the $v_8 \le 2$ data. Previous ν_4 data from Ref. [5].

[b] Initially incorrectly given as 19 [2] because one line with $K = 20$ was overlooked.

[c] These numbers were initially [2] interchanged.

[d] Each blend of lines counted as one line. Hyperfine splitting in present and previous data was considered in the present fit. Transitions with $K = 0$ of l-doubled states associated with $v_8 = 1^{-1}$ and $v_8 = 2^{+2}$, respectively, in present data set. Lines, which were weighted out, are not counted. Transitions between vibrational states counted for higher vibrational state.

[e] No rms error was given in Refs. [5]; we assume parameter uncertainties are based on standard errors, i.e. the rms error is 1.0 by definition. No rms value was given in that work for the rotational data.

[f] No individual $\Delta K = 3$ loops were given in Ref. [30]. We used the five $\Delta K = 3$ splittings from Table II in that work with the reported uncertainties.

Table 3: Transition dipole moments μ (D), Herman-Wallis correction μ_{HW}[a] (D), and integrated intensities I_H[b] (10^{-19} cm/molecule) of IR bands of CH_3CN calculated using the present Hamiltonian model together with the extrapolated and experitentally measured total integrated intensities from previous studies.

			Integrated intensity				
band	μ	μ_{HW}	I_H	[49]	[50]	[51]	[52]
ν_4[c]	0.023	−0.0022	2.028	1.95	1.93	2.30	2.06
$2\nu_8$[d]	0.030		2.580	2.63	2.50	3.43	
ν_8[d]	0.043		2.285		1.77	1.81	2.79

[a] First-order Herman-Wallis correction; coefficient of $i(\{\phi_c, J_b\} - \{\phi_b, J_c\})/2$.

[b] Estimated from the cold bands, $v_4 = 1 - 0$, $v_8 = 2 - 0$ and $1 - 0$, by multiplication with the vibrational partition factor 1.5006 at 296 K. An increase of 2.677 % from other isotopic species was considered.

[c] μ, μ_{HW}, and I_H from this work.

[d] μ and I_H from Ref. [2]; μ_{HW} was not needed. Please note that the transition dipole moments in Ref. [2] were given correctly in the text, but were a factor of 10 too large in Table 10.

Nevertheless, two P-branch transitions were assigned unambiguously that had sufficient intensities and appeared to be not blended with other lines. **Fig. 8** shows the $P(8)$ transitions of ν_4 together with $P(15)$ transitions of $\nu_4 + \nu_8 - \nu_8$. The assignments in ν_4 cover the entire range of the line list which was truncated at the high end because of the weakness of the ν_4 lines and the onset of ν_7 and at the low end by the overlap with the ν_3 band of OCS. Even though the Q-branch was rather compact, many lines up to $J = 42$ and $K = 13$ were isolated or occured as sufficiently narrow groups of lines to permit inclusion in the fit. Uniform uncertainties of 0.0001 cm^{-1} were attributed to the lines, even though this may be somewhat conservative for parts of the stronger lines. Statistics to this data set can be found in **Table 2**.

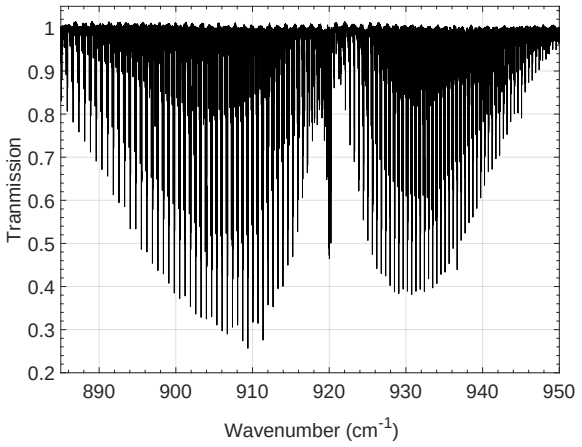

Figure 7: Overview of the ν_4 band of CH_3CN. The strong ν_3 band of OCS becomes prominent at lower wavenumbers. A small amount of OCS was added for calibration purpose, see section 2.3.

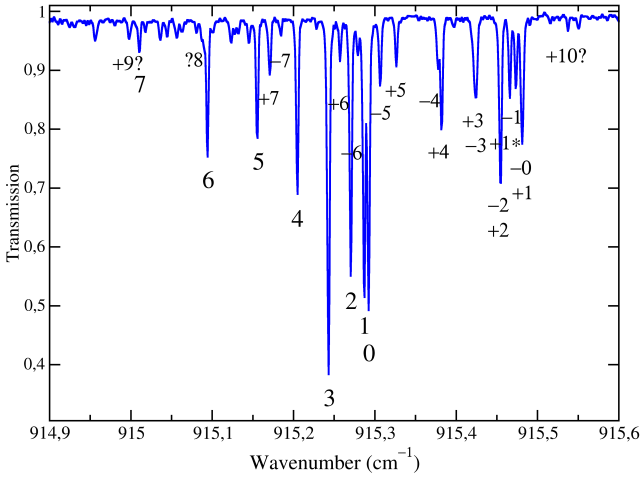

Figure 8: Section of the ν_4 band of CH_3CN showing the $J = 7-8$ transitions of ν_4 and $J = 14-15$ transitions of $\nu_4+\nu_8-\nu_8$. The K quantum numbers are given centered below each line for ν_4; $k = K \times l$ is given in the case of $\nu_4 + \nu_8 - \nu_8$. Question marks indicate tentative assignments for $k = +9$ and $+10$; for $K = 8$, it indicates that the K value is quite certain, but not if it is $l = +1$ or, more likely, $l = -1$. Please note that $J = 13 - 14$ for the tentative $k = +10$ transition. Unassigned transitions are probably due to $\nu_4 + 2\nu_8 - 2\nu_8$.

The amount of CH_3CN in the ground vibrational state can be evaluated from the partial pressure of methyl cyanide by subtracting off the contributions of other isotopic species and taking into account the vibrational factor of CH_3CN at 291 K. However, a Herman-Wallis correction had to be evaluated also because the P-branch is considerably stronger than the R-branch. A transition dipole moment of 0.023 D combined with −0.0022 D as the coefficient of $i(\{\phi_c, J_b\} - \{\phi_b, J_c\})/2$ as first-order Herman-Wallis correction reproduced the band shape sufficiently well. These values and the resulting integrated band strength determined in this study is given in **Table 3** together with our earlier values for ν_8 and $2\nu_8$ [2] and band strength data from previous studies. The line intensities are modeled very well around the P- and R-branch maxima. The intensities are slightly small at low J in the R-branch and at high J in the P-branch, whereas they are slightly high at low J in the P-branch and at high J in the R-branch, or, in other words, the present Herman-Wallis correction is slightly too small at low J and slightly too large at high J. There is no appropriate correction available in SPCAT to the best of our knowledge to reduce these small, albeit systematic deviations. The ν_4 intensities did not show any significant intensity deviations with K. We point out that the same dipole parameters reproduce the $\nu_4 + \nu_8 - \nu_8$ intensities well, as is usually the case.

3.3. The $v_8 = 2$ state

3.3.1. Rotational data and analysis

The $v_8 = 2$ rotational data in the present study were taken to a large extent from our previous investigation [2]. These data comprise parts of earlier data, $J'' = 0$, 4, and 5 from Ref. [53] and $J'' = 19$ from Ref. [20].

In the course of recording transitions pertaining to $v_4 = 1$ at 2 and 1 mm, we also covered $v_8 = 2$ transitions in this region to test the impact in the fit. This was partially based on the fact that the presently calculated uncertainties of transitions of $v_8 = 2^{-2}$, $K = 2$ and of $v_8 = 2^0$, $K = 4$ had larger uncertainties than those of most other transitions in $v_8 = 2$, and these uncertainties were large enough to warrant measurement. These larger uncertainties were caused by the q_{22} interaction between these two K levels with a crossing at $J = 40$. Interestingly, transitions connecting these two different K ladders had sufficient intensities between $J'' = 8$ and 12 that they could be recorded with fairly good S/N. These cross-ladder transitions were comparatively strong far away from the resonance because the mixing coefficients for these J levels change much more than for two successive J levels closer to the resonance, where the mixing coefficients are almost constantly close to 0.5. These transition frequencies together with the remaining lines recorded in the 2 and 1 mm regions accounted for a considerable part of the improved $v_8 = 2$ parameters, in particular those of lower order.

Further measurements in the 770−1086 GHz region were mostly carried out to improve the coverage of interactions with $v_8 = 1$ and 3 and with $v_4 = 1$ through new or more accurate measurements. The interactions with $v_4 = 1$ were already described in Section 3.2.1.

There is a Fermi resonance between $v_8 = 1^{-1}$ and $v_8 = 2^{+2}$ with the largest perturbations in $K = 14$ and a crossing between $J = 91$ and 92. Perturbations from this resonance are smaller at $K = 13$ and even smaller at other K. We added several new or remeasured transitions with $41 \le J'' \le 58$ and $K = 13$ to 15 in both vibrational substates. The highest J'' value for these K was 64 from our previous study [2].

There are, however, additional resonances, which perturb the $K = 13$ levels of both vibrational substates, and which are described by $\Delta v_8 = \pm1$, $\Delta K = \mp2$, $\Delta l = \pm1$. $K = 13$ of $v_8 = 1^{-1}$ interacts with $K = 11$ of $v_8 = 2^0$ with a crossing near $J = 60$. All four strong transitions were observed earlier [2]; the transitions with $J'' = 59$ are between the two vibrational states. Several further $K = 11$ lines of $v_8 = 2^0$ were recorded in addition. $K = 13$ of $v_8 = 2^{+2}$ interacts with $K = 15$ of $v_8 = 1^{+1}$; a crossing occurs between $J = 52$ and 53. Of the 8 relatively strong transitions perturbed most, the transition with $J'' = 51$ to 53 within each vibrational substate and the fairly strong cross-ladder transitions with $J'' = 52$, only the $J'' = 51$ with $K = 15$ of $v_8 = 1^{+1}$ is not in our line list. Three transitions were recorded newly and two were remeasured.

Further resonances exist between $v_8 = 2$ on one hand and $v_8 = 3$ or $v_7 = 1$ on the other hand. There is a Fermi resonance between $v_8 = 2^0$ and $v_8 = 3^{+3}$ at $K = 14$ and, more pronounced, at $K = 15$ with a crossing currently calculated between $J = 73$ and 74. The previous lines in $v_8 = 2^0$ extended to $K = 13$, and only one line each was added to $K = 12$ and 13. Additional Fermi resonances are found between $v_8 = 2^{-2}$ and $v_8 = 3^{+1}$ at $K = 12$ and 13 and between $v_8 = 2^{-2}$ and $v_7 = 1^{+1}$ at $K = 13$ and 14. Transitions in $v_8 = 2^{-2}$ extend to $K = 11$, and four lines were added to this K among others. Several $\Delta K = \mp2$, $\Delta l = \pm1$ interactions were noticed, but their effects were not yet strong enough to warrant treatment in the fit.

The change in $v_8 = 2$ parameter values in the course of the present investigation and in particular caused by the lines around the $v_8 = 2/v_4 = 1$ resonances resulted in additional parameter constraints and unconstraining another pair of parameters. Since ΔD_K of $v_8 = 2^0$ and $v_8 = 2^2$ were the same within three times the comparatively large uncertainty of the latter, the two parameters were constrained to be the same, essentially without deterioration of the quality of the fit. The resulting $\Delta D_K(v_8 = 2)$ was identical to two times $\Delta D_K(v_8 = 1)$ well within the larger uncertainty of the latter. Therefore, the ratio of 2 : 1 was constrained. Subsequently, the values of η_K and q_K of $v_8 = 2$ were contrained to be identical to the respective $v_8 = 1$ values with only a marginal deterioration of the fit. A slight improvement was achieved by decoupling η_{JK} of $v_8 = 1$ and 2. The mutually constrained parameters $F_{2,J}(8^{\pm1}, 8^{2,0})$ and $F_{2,J}(8^{\pm1}, 8^{2,\pm2})$ were introduced to the fit as a result of the improved data situation.

In the course of these analyses, two very weak $2\nu_8$ lines, ${}^oR_9(38)$ and ${}^oR_9(43)$, were found to deviate from their calculated positions by ∼11 times the attributed uncertainties of 0.0003 cm^{-1} and were omitted. Also omitted was the ${}^oR_7(41)$ line with a residual slightly more than three times the uncertainty. Two high-K rotational lines were omitted which were already weighted out because of their large residuals, $J'' = 23$, $K = 13$ of $v_8 = 2^0$ and $J'' = 55$, $K = 15$ of $v_8 = 2^{+2}$. Two more lines, $J'' = 55$, $K = 14$ and $J'' = 53$, $K = 15$ of $v_8 = 2^{+2}$, with somewhat large residuals were omitted after inspection of their intensities and their line shapes. Statistics to the $v_8 = 2$ rotational data sets are given in **Table 2**. Please note that the maximum K values of $v_8 = 2^0$ and $v_8 = 2^{+2}$ were exchanged erroneously in our previous study [2].

3.3.2. The $2\nu_8$ band

The $2\nu_8$ data were initially taken from our previous study [2], but with three lines omitted as described in Section 3.3.1. We scrutinized the $2\nu_8$ line positions and corrected about half of the $2\nu_8^0$ position because these were from the initial calibration and assignments and were on average ∼0.0002 cm^{-1} lower compared to the final calibration. A small number of transition frequencies with large residuals were corrected or were omitted because of blending with unknown transitions. The uncertainties of parts of the $2\nu_8^0$ Q-branch and $2\nu_8^{\pm2}$ lines were reevaluated and additional assignments were made which, most notably, included 5 $2\nu_8^0$ Q-branch transitions with $K = 13$. These changes affected the parameter values and uncertainties fairly little, but reduced the rms and rms errors of the $2\nu_8$ data sets. Isolated lines with sufficiently good S/N were given uncertainties of 0.0002 cm^{-1} as previously. Noisier lines or lines in more crowded regions, such as in the Q-branch, were often given larger uncertainties of 0.0003 cm^{-1} to 0.0010 cm^{-1}. The J and K ranges and other information on this data set are given in **Table 2**. The quality of the data in our present fit is better than that in our previous fit, but still slightly worse than in the original study, in which 0.12, 0.18, and 0.18×10^{-3} cm^{-1} were reported for $2\nu_8^0$, $2\nu_8^{+2}$, and $2\nu_8^{-2}$, respectively from the IR + MW fit [54].

3.4. The $v_8 = 1$ state

3.4.1. Rotational data and analysis

The $v_8 = 1$ rotational data in the present study were taken for the most part from our previous investigation [2]. These data comprise parts of earlier data, $J'' = 3$ to 7 from Ref. [55] and $k \times l = +1$ direct-l-type transitions from Refs. [56] and [57].

New transition frequencies involving the $v_8 = 1$ and 2 interaction were mentioned in Section 3.3.1. The impact of transition frequencies with $J'' = 9$ and $K \leq 5$ was marginal in spite of uncertainties of mostly 3 or 5 kHz. We also determined new transition frequencies involving the $v_8 = 0$ and 1 interaction. These were remeasurements of the $J'' = 42$ and 43 transitions of $v_8 = 0$, $K = 14$ and $v_8 = 1^{+1}$, $K = 12$, measurement of one of the two $J'' = 42$ cross-ladder transitions and remeasurement of one of the two $J'' = 43$ cross-ladder transitions. Statistics to the $v_8 = 1$ rotational data sets are given in **Table 2**. Please note that the maximum K value of $v_8 = 1^{+1}$ was increased from 19 to 20 with respect to our previous study [2] because we overlooked the previously recorded $J'' = 60$ transition in the course of analyzing the fit statistics.

3.4.2. The ν_8 band

Transition frequencies of ν_8 were taken from Ref. [58] without any change with respect to our previous study [2]. Briefly, almost all fully weighted lines were assigned uncertainties of 0.0002 cm^{-1}, 0.0004 cm^{-1} for a small number of weak lines and 0.0006 cm^{-1} for lines with weight 0.1. The J and K ranges and other information on this data set are given in **Table 2**. The quality of the data in our present and previous fits are about the same and only slightly worse than in the original study in which 0.17 and 0.16×10^{-3} cm^{-1} were reported for ν_8^{+1} and ν_8^{-1}, respectively from the IR + MW fit.

3.5. The $v = 0$ state

The $v = 0$ data are identical to those of our previous investigation [2] with the exception of the new transition frequencies involving the $v_8 = 0$ and 1 interaction mentioned in Section 3.4.1. The previous data consist of Lamb-dip measurements covering parts of $J'' = 4$ to 42 from 91 to 780 GHz [59], terahertz data with $59 \leq J'' \leq 81$ between 1.09 and 1.51 THz [2] and with $J'' = 86$ to 88 near 1.6 THz [27]. Also included were perturbed $K = 14$ transitions mostly from Ref. [2] and from Ref. [60] as well as hyperfine split transitions with $J'' = 0$ [61], $J'' = 1$ [62], and $J'' = 2$ and 7 [63]. Direct information on the axial parameters come from five ground state combination loops with $K = 3 - 0$ to $7 - 4$ which were averaged over several different J [30]. Trial fits with these parameters floated showed that the they still differed somewhat from our previous values [2]. But these differences were deemed to be small enough to keep these parameters floated, even more so, as their uncertainties improved substantially with respect to those in [2]. Fit statistics are again provided in **Table 2**.

3.6. The global fit up to $v_4 = 1$

Our global fit of low-lying vibrational states of methyl cyanide up to $v_8 = 2$ was extended to include $v_4 = 1$, as de-

Table 4: Present spectroscopic parameters or differences Δ thereof [a,b] (cm^{-1}, MHz)[c] of methyl cyanide within vibrational states $v = 0$ and $v_4 = 1$ in comparison to previous values.

	$v = 0$		$v_4 = 1$	
Parameter X	Present	Ref. [2]	Present	Ref. [5]
E_{vib}[c]	0.0	0.0	920.290464 (5)	920.290284 (13)
(Δ)[b] $(A - B)$	148900.011 (38)	148900.103 (66)	−165.941 (14)	−166.205 (33)
(Δ)[b] B	9198.899163 (10)	9198.899167 (11)	−46.14784 (5)	−46.14822 (66)
(Δ)[b] $D_K \times 10^3$	2827.9 (6)	2830.6 (18)	−25.13 (26)	−31.63 (63)
(Δ)[b] $D_{JK} \times 10^3$	177.40780 (25)	177.40787 (25)	7.130 (5)	7.165 (17)
(Δ)[b] $D_J \times 10^6$	3807.572 (7)	3807.576 (8)	−5.510 (24)	−5.702 (99)
(Δ)[b] $H_K \times 10^6$	156.2 (20)	164.6 (66)	15.5 (12)	−22.2 (28)
(Δ)[b] $H_{KJ} \times 10^6$	6.0618 (14)	6.0620 (14)	−11.705 (95)	−13.895 (105)
(Δ)[b] $H_{JK} \times 10^9$	1025.62 (14)	1025.69 (15)	244.7 (13)	315.7 (33)
(Δ)[b] $H_J \times 10^{12}$	−238.7 (20)	−237.4 (21)	150.3 (29)	
(Δ)[b] $L_{KKJ} \times 10^9$	−0.4441 (25)	−0.4443 (25)	−23.85 (69)	
(Δ)[b] $L_{JK} \times 10^{12}$	−52.65 (51)	−52.75 (51)	78.7 (15)	
(Δ)[b] $L_{JJK} \times 10^{12}$	−7.876 (31)	−7.901 (32)	−3.51 (16)	
(Δ)[b] $L_J \times 10^{15}$	−3.00 (16)	−3.10 (17)		
(Δ)[b] $P_{KKJ} \times 10^{12}$			−24.3 (16)	
(Δ)[b] $P_{KJ} \times 10^{12}$			2.482 (43)	
(Δ)[b] $P_{JK} \times 10^{15}$	0.507 (67)	0.552 (68)	−50.1 (14)	
(Δ)[b] $P_{JJK} \times 10^{18}$	53.9 (21)	55.3 (22)		
(Δ)[b] eQq	−4.22297 (103)	−4.22308 (107)		
(Δ)[b] $C_{bb} \times 10^3$	1.840 (89)	1.845 (90)		
(Δ)[b] $(C_{aa} - C_{bb}) \times 10^3$	−1.17 (30)	−1.15 (31)		

[a] Numbers in parentheses are one standard deviation in units of the least significant figures. Empty entries indicate parameters not applicable or not used in the fit. See Ref. [2] for sign and value considerations.

[b] Parameter X given for $v = 0$; $\Delta X = X_i - X_0$, with i representing an excited vibrational state.

[c] All parameters given in units of megahertz, except for E_{vib}, which is given in units of inverse centimeters.

scribed in Section 3.2, supplemented by additional data pertaining to lower vibrational states and minor omissions as detailed in Sections 3.3, 3.4, and 3.5. As in our previous work [2], our fit takes into account states up to $v_8 = 3$. This truncation will have some effect on the parameter values of $v_8 = 2$ and $v_4 = 1$; $v_8 = 0$ and 1 should be affected to a much lesser extent. Transition frequencies with large residuals were retained in the fit if they may be caused by insufficiently accounted perturbations, but were usually weighted out. The rms error of the global fit is 0.853, slightly below 1.0. Details on separate data sets along with additional fit statistics are given in **Table 2**. We also state the rms values, which are often given as only information on the quality of the fit. These values are useful if all or most of the uncertainties are the same and the spread of the uncertainties is not more than a factor of a few. This applies to most of the separate IR data sets, but not to the rotational data sets as in these cases the uncertainties differ by around a factor of 100. The rms is then dominated by transitions with relatively large residuals.

Similar to our previous work, we provide the spectroscopic parameters of our global fit in several tables. In all instances, these are compared to previous values. These were taken from Ref. [2] for $v_8 \leq 2$ and Ref. [5] for $v_4 = 1$. Parameters for $v_7 = 1$ and $v_8 = 3$ were taken from the latter work as well; the small number of $v_8 = 3$ parameters determined or adjusted in the present study are given in separate rows. Previous interaction parameters were taken from one of the two references. The ground state and $v_4 = 1$ parameters are listed in **Table 4**, $v_7 = 1$ and $v_8 = 3$ parameters in **Table 5**, interaction parameters in **Table 6**, and $v_8 = 1$ and 2 parameters are given in **Table 7**. The line, parameter, and fit files are available as supplementary material. They will also be provided in the Cologne Spectroscopy Data section of the CDMS[2]. Calculations of the rotational ($v_4 = 1$) and rovibrational (ν_4) spectra will be deposited in the catalog section of the CDMS[3].

3.7. Single state analysis of $v_4 = v_8 = 1$

The ν_4 IR spectrum contained numerous unassigned features which displayed fairly regular patterns for which the assignment to the $\nu_4 + \nu_8 - \nu_8$ hot band suggested itself. Transitions originating in $v_8 = 1$ are exactly a factor of 6 weaker than corresponding transitions in $v = 0$ at 293 K. Combining the $v_4 = 1$ vibrational changes with the complete set of $v_8 = 1$ parameters, which are the $v = 0$ parameters, the $v_8 = 1$ vibrational changes and intravibrational Coriolis- and q_{22}-derived parameters, and all appropriate hyperfine parameters, yielded good estimates of the $v_4 = v_8 = 1$ parameters. From these, numerous transitions could be assigned tentatively or with certainty in the $\nu_4 + \nu_8 - \nu_8$ hot band. Uncertainties of 0.0002 or 0.0004 cm^{-1} were assigned to most hot band transitions for isolated lines with good S/N and other lines, respectively, compared to the smaller 0.0001 cm^{-1} in the ν_4 cold band, because of many perturbations, in particular at higher K, and because lines are frequently close to other lines, as can be seen in **Fig. 8**. Transition

[2] https://cdms.astro.uni-koeln.de/classic/predictions/daten/CH3CN/CH3CN/
[3] https://cdms.astro.uni-koeln.de/

Table 5: Spectroscopic parameters or differences Δ thereof [a,b] (cm^{-1}, MHz)[c] of methyl cyanide within vibrational states $v_7 = 1$ and $v_8 = 3$ mostly taken from Ref. [5].

Parameter X	$v_7 = 1$	$v_8 = 3^1$	$v_8 = 3^3$
$E_{\rm vib}$[c]	1041.85471	1077.7863	1122.15
$E_{\rm vib}$[c,d]		1077.7919 (2)	1122.3489 (1)
$\Delta(A-B)$	889.440	−302.030	−347.76
$\Delta(A-B)$[d]			−442.16 (6)
ΔB	−5.73413	80.29485	81.289
ΔB[d]			80.6130 (13)
$\Delta D_K \times 10^3$	149.333	−22.8[e]	−22.8[e]
$\Delta D_K \times 10^3$[d]		−30.6[e]	−30.6[e]
$\Delta D_{JK} \times 10^3$	0.9731	3.5046[e]	3.5046[e]
$\Delta D_J \times 10^6$	14.001	462.[e]	462.[e]
$\Delta H_{JK} \times 10^9$	−148.1		
$A\zeta$	66663.668	138665.87	138527.8
$A\zeta$[d]		138656.0	138654.7
η_K	7.2248	11.013[e]	11.013[e]
η_J	0.078153	0.40154[e]	0.40154[e]
$\eta_{KK} \times 10^6$	64.8		
$\eta_{JK} \times 10^6$	−50.34		
$\eta_{JJ} \times 10^6$	2.385	7.285[e]	7.285[e]
q	4.7634	17.683[e,f]	17.683[e,f]
$q_J \times 10^6$	−10.85	−75.79[e,f]	−75.79[e,f]

[a] Empty entries indicate parameters not applicable or not used in the fit. Signs of q and q_J altered, see Ref. [2].

[b] Parameter difference $\Delta(X) = X_i - X_0$, given for rotational and distortion parameters (i represents an excited vibrational state).

[c] All parameters given in units of megahertz, except for $E_{\rm vib}$, which is given in units of inverse centimeters.

[d] Value determined or estimated in the present work, see also Section 3.2.1.

[e] Ratio kept fixed in the fit for parameter X or ΔX.

[f] The parameter q and its distortion corrections connect levels with $\Delta K = \Delta l = 2$, see subsection 3.1 and Ref. [2].

Table 6: Present and previous interaction parameters[a] (MHz) between low-lying vibrational states of methyl cyanide.

Parameter	Present	Ref. [2]
$F_2(0, 8^1) \times 10^3$	−70.9033 (44)	−70.897 (27)
$F(8^{\pm1}, 8^{2,\mp2})$	53137.8 (19)	53157.7 (33)
$F_K(8^{\pm1}, 8^{2,\mp2})$	−6.[b,c]	−6.[b,c]
$F_J(8^{\pm1}, 8^{2,\mp2}) \times 10^3$	−370.42 (30)[b]	−369.89 (44)[b]
$F_{JJ}(8^{\pm1}, 8^{2,\mp2}) \times 10^6$	1.389 (63)[b]	1.681 (87)[b]
$F_2(8^{\pm1}, 8^{2,0}) \times 10^3$	−62.32 (31)[d]	−65.491 (24)[d]
$F_2(8^{\pm1}, 8^{2,\pm2}) \times 10^3$	−124.64 (63)[d]	−130.982 (48)[d]
$F_{2,J}(8^{\pm1}, 8^{2,0}) \times 10^6$	−1.11 (10)[e]	
$F_{2,J}(8^{\pm1}, 8^{2,\pm2}) \times 10^6$	−2.21 (21)[e]	
$F_{ac}(8^{2,\pm2}, 4^1)$ [$2w_{488}$]	8.76557 (13)	8.7362 (21)
$F_{2ac}(8^{2,0}, 4^1) \times 10^6$	−6.941 (9)	−7.98 (16)
$F(8^{2,\pm2}, 7^{\mp1})$ [W_{788}]	45170.8[f]	45170.8[f]
$F(8^{2,\pm2}, 8^{3,\mp1})$	75985. (66)	77208. (93)
$F(8^{2,0}, 8^{3,3})$	90876. (47)	91509. (131)
$G_b(4, 7)$ [$2W_{47}$]	909.[f]	909. (2)[f,g]
$F_{bc}(4, 7)$ [$2w_{47}$]	−1.9325 (22)	−1.84 (2)[f,g]
$F(4, 8^{3,\pm3})$ [W_{4888}]	11381.1 (16)	11430. (6)[f,g]
$F_J(4, 8^{3,\pm3}) \times 10^3$	56.85 (38)	
$F_2(4, 8^{3,\pm1}) \times 10^3$	116.8 (16)	
$F_{2J}(4, 8^{3,\pm1}) \times 10^6$	−7.50 (91)	
$F_4(4, 8^{3,\mp1}) \times 10^6$	−2.53 (13)	
$F(7^{\pm1}, 8^{3,\pm1})$ [W_{7888}]	50129.2[f]	50129.2[f]
$G_a(7^{\pm1}, 8^{3,\pm1})$ [$2W^k_{7888}$]	−2239.1[f]	−2239.1[f]

[a] Alternative designations from Ref. [5] given in brackets. Numbers in parentheses after the interaction parameter designate the vibrational states separated by a comma, see also Ref. [2]. Numbers in parentheses after the values are one standard deviation in units of the least significant figures.

[b] J and K distortion corrections to $F(8^{2,\pm2}, 8^{3,\mp1})$ and $F(8^{2,0}, 8^{3,3})$ kept fixed to $\sqrt{2}$ and $\sqrt{3}$, respectively, times the corresponding $F(8^{\pm1}, 8^{2,\mp2})$ value; see, e.g., Ref. [9].

[c] Estimated assuming $F_K/F_J \approx A/B$, see Ref. [2].

[d,e] Ratios constrained, see Ref. [2].

[f] Kept fixed to values from Ref. [5].

[g] Uncertainties reported in Ref. [5].

Table 7: Spectroscopic parameters or differences Δ thereof [a,b] (cm^{-1}, MHz)[c] of methyl cyanide in its $v_8 = 1$ and 2 states in comparison to previous values.

	$v_8 = 1$		$v_8 = 2^0$		$v_8 = 2^2$	
Parameter X	Present	Ref. [2]	Present	Ref. [2]	Present	Ref. [2]
E_{vib}[c]	365.024349 (7)	365.024365 (9)	716.749852 (49)	716.75042 (13)	739.147650 (34)	739.148225 (56)
$\Delta(A-B)$	−115.871 (10)	−115.930 (26)	−187.539 (16)	−187.404 (18)	−260.109 (26)	−259.956 (122)
ΔB	27.53032 (4)	27.53028 (5)	54.05757 (6)	54.05732 (11)	54.50276 (4)	54.50273 (7)
$\Delta D_K \times 10^3$	−10.21 (9)[d]	−11.46 (48)	−20.42 (17)[d]	−20.2 (3)	−20.42 (17)[d]	−7.5 (16)
$\Delta D_{JK} \times 10^3$	0.9892 (5)	0.9875 (6)	1.6657 (11)	1.6755 (25)	1.8036 (10)	1.8088 (15)
$\Delta D_J \times 10^6$	95.999 (13)	95.599 (17)	216.372 (27)	216.319 (37)	189.151 (22)	189.162 (31)
$\Delta H_K \times 10^6$	20.8 (5)	14.9 (22)				
$\Delta H_{KJ} \times 10^9$	43.1 (19)[d]	34. (2)	86.2 (37)[d]	150. (24)	86.2 (37)[d]	25. (6)
$\Delta H_{JK} \times 10^9$	2.58 (6)	2.59 (6)	14.09 (18)	17.71 (34)	1.93 (12)	−0.37 (21)
$\Delta H_J \times 10^{12}$	317.8 (25)	315.3 (30)	208.1 (51)	200.7 (63)	631.3 (48)	627.8 (59)
$\Delta L_J \times 10^{15}$	−2.82 (17)[d]	−2.64 (20)[d]	−5.64 (35)[d]	−5.28 (40)[d]	−5.64 (35)[d]	−5.28 (40)[d]
$\Delta(eQq)$[d]	−0.0391 (19)[d]	−0.0387 (19)[d]	−0.0782 (38)[d]	−0.0774 (38)[d]	−0.0782 (38)[d]	−0.0774 (38)[d]
$eQq\eta$	0.1519 (113)	0.1519 (113)				
$A\zeta \times 10^{-3}$	138.65600 (5)	138.65620 (7)			138.65535 (6)	138.65604 (10)
η_K	10.311 (3)[d]	10.333 (7)			10.311 (3)[d]	10.405 (10)
η_J	0.390457 (5)	0.390469 (7)			0.394523 (4)	0.394512 (6)
$\eta_{KK} \times 10^6$	−677. (18)[d]	−834. (41)[d]			−677. (18)[d]	−834. (41)[d]
$\eta_{JK} \times 10^6$	−33.91 (6)	−34.06 (6)[d]			−34.66 (6)	−34.06 (6)[d]
$\eta_{JJ} \times 10^6$	−2.3668 (12)[d]	−2.3595 (24)[d]			−2.3668 (12)[d]	−2.3595 (24)[d]
$\eta_{JKK} \times 10^9$	2.20 (17)[d]	2.59 (17)[d]			2.20 (17)[d]	2.59 (17)[d]
$\eta_{JJK} \times 10^9$	0.511 (5)[d]	0.509 (6)[d]			0.511 (5)[d]	0.509 (6)[d]
q	17.798485 (24)	17.798438 (23)	[e]	[e]	17.73001 (8)[e]	17.72986 (14)[e]
$q_K \times 10^3$	−2.6290 (50)[d]	−2.6645 (111)	[e]	[e]	−2.6290 (50)[d,e]	−2.6153 (89)[e]
$q_J \times 10^6$	−63.861 (14)	−63.842 (14)	[e]	[e]	−68.719 (22)[e]	−68.668 (31)[e]
$q_{JK} \times 10^9$	93.35 (45)[d]	93.19 (53)[d]	[e]	[e]	93.35 (45)[d,e]	93.19 (53)[d,e]
$q_{JJ} \times 10^{12}$	309.9 (14)	311.5 (15)	[e]	[e]	197.1 (21)[e]	191.9 (26)[e]

[a] Numbers in parentheses are one standard deviation in units of the least significant figures. Empty entries indicate parameters not applicable or not used in the fit. See Ref. [2] for sign and value considerations.

[b] Parameter difference $\Delta(X) = X_i - X_0$ given for rotational and distortion parameters (i represents an excited vibrational state).

[c] All parameters given in units of megahertz, except for E_{vib}, which is given in units of inverse centimeters.

[d] Ratio kept fixed in the fit for respective X or ΔX.

[e] The parameter q and its distortion corrections connect levels with $\Delta K = \Delta l = 2$, see subsection 3.1 and Ref. [2].

frequencies with large residuals and tentative assignments were weighted out. Ultimately, assignments in the *R*- and *P*-branch extended to $J' = 43$ and 49, respectively. A small number of assignments were also made in the *Q*-branch, notably transitions with $k = K \times l = +7$ and $J = 7$ to 10.

Transitions with $K \leq 4$ and $k = +5$ appear to be largely unperturbed and could be fit within the currently assigned uncertainties. However, some *R*-branch transitions with $k = -2$, -3, -4, and $+4$ had small, but systematic deviations for a few J. They were weighted out if the deviations were considerably larger than the uncertainties. All other k values appear to be perturbed by different degrees. An additional feature of the $\nu_4 + \nu_8 - \nu_8$ hot band is, that transitions having the same K and opposite l occur frequently close to each other; in the *P*-branch, e.g., $K = 2$, 3, and 4, see **Fig. 8**. The $k = -5$ lines are all nearly constantly about 0.015 cm^{-1} lower than calculated, whereas the $k = -6$ lines are shifted in the opposite direction by around 0.03 cm^{-1}. These perturbations are caused, at least in part, by anharmonic resonances with $v_7 = v_8 = 1^{+2}$ and $v_8 = 4^{+2}$, as was observed for $CH_3C^{15}N$ [25]. The latter resonances corresponds to the $v_4 = 1/v_8 = 3$ resonance discussed in Section 3.2.1, but was not considered in the analysis in Ref. [6], most likely caused by the lack of data in $v_4 = v_8 = 1$ and in $v_8 = 4^2$. The resonance with $v_7 = v_8 = 1^{+2}$, however, was included in their model. A pronounced change in the $k = -6$ residuals may be caused in addition by an interaction with the higher lying $K = 4$ levels of $v_7 = v_8 = 1^0$. The origin of the residuals in $k = -7$ are less clear. They may still be caused by the two anharmonic resonances affecting $k = -5$ and -6. They may also be caused by $\Delta K = -1$, $\Delta l = +2$ interaction with $v_6 = 1$, which was included in the analysis of Ref. [6], for which the K levels are closest at $K = 10$ and 9, respectively. The $k = -7$ lines appear to be blended in the *P*-branch with the stronger $k = +7$ lines around $J'' = 35$ and are shifted increasingly up with decreasing J noticeably starting at $J'' = 32$. The shift is 0.011 cm^{-1} at $J'' = 15$ in **Fig. 8**. The transitions with $k = +6$ and $+7$ are shifted down by about 0.0015 and 0.008 cm^{-1}, respectively, with essentially no change in J, almost certainly caused by an anharmonic resonance with $v_8 = 4^{+4}$, as observed for $CH_3C^{15}N$ [25] and again equivalent to the $v_4 = 1/v_8 = 3$ resonance discussed in Section 3.2.1. This resonance should push up levels with $k = +8$, as in the case of $CH_3C^{15}N$. We identified transitions with the correct intensity for $k = +8$ or $k = -8$; these transitions should have the same intensity. They are, however, lower in frequency than calculated, thus possibly favoring the assignment to $k = -8$. At any rate, one series of $K = 8$ transitions appears to be shifted by amounts which make it difficult to identify these transitions at present. Some very tentative assignments were made for $k = +9$ and $+10$. Even transitions having $k = -11$ and possibly -9 and -10 may be assignable eventually. It is not only the presumably large perturbations in these levels which make assignments difficult so far, but also the amount of unassigned transitions with similar or even higher intensities, as can be noted in **Fig. 8**. These transitions belong most likely to the $\nu_4 + 2\nu_8 - 2\nu_8$ hot band, which is a factor of 36 weaker than ν_4 and a factor of six weaker than $\nu_4 + \nu_8 - \nu_8$. Transitions of $2\nu_4 - \nu_4$ or of the ν_4 bands of the two methyl cyanide isotopologs with one ^{13}C could complicate the situation further as these are less than a factor of 100 weaker than ν_4 of the main isotopolog.

From these IR transition frequencies, some small corrections $\Delta\Delta X := X_{4,8} - \Delta X_4 - \Delta X_8$ could be determined; $\Delta X_4 := 0$ if the parameter X is not defined for $v_4 = 0$ and 1. Rotational transitions above 440 GHz could be assigned subsequently up to 1.2 THz. Lower frequency transitions were measured later. **Fig. 9** displays a large part of the $J = 14-13$ transitions. The assignments were straightforward and are considered to be secure for K series that appeared to be unperturbed or only slightly perturbed. More strongly perturbed transitions could be assigned with confidence quite often taking into account relative intensities and trends in the deviations, however it may be that blending of some lines escaped notice. Caution is advised if the deviations display complex patterns, in particular if they are quite different for a small number of transitions. We mention in the following only interactions that did not show up in the IR data because of their small effects or because of the absence of data.

Transitions in $v_4 = v_8 = 1^{+1}$ appear to be not or only slightly perturbed, less than ~0.3 MHz for $1 \leq K \leq 5$, and the coverage is good with ~30 transitions up to mostly $J'' = 64$. The coverage is also good for $K = 6$ to 8. $K = 6$ is only slightly perturbed, less than 1 MHz up to $J'' = 53$ and slightly more than 3 MHz for $J'' = 64$. Transitions with $K = 7$ are shifted slightly down at low J, then up for $J'' = 18$ to 44 or 55, then decreasing again for still higher J. An assignment of a line 67 MHz higher than calculated for $J'' = 53$ is uncertain. Transitions with $K = 8$ are shifted decreasingly up for $J'' \leq 16$ and then down by up to ~130 MHz for $J'' = 49$. The assignment of $J'' = 60$ to a line close to the prediction is very tentative and appears to require that the $J'' = 61$ and 63 lines are blended with the respective lines of $v_4 = v_8 = 1^{-1}$ with $K = 3$ and 2, respectively, or shifted so much that they could not be assigned with confidence. The perturbations in $K = 6$ to 8 are caused at least in part by an anharmonic resonance with $v_8 = 4^{+4}$, as mentioned further up in this section. Additional perturbations in $K = 7$ may be caused by $K = 8$ of $v_8 = 3^{-1}$, which is only ~0.7 cm^{-1} higher at low J, and by $K = 6$ of $v_8 = 3^{-3}$, which crosses $K = 7$ between $J = 20$ and 21 according to current calculations. These resonances are analogous to $v_4 = 1/v_8 = 2^{-1}$ interactions mentioned in Section 3.2.1. Further perturbations in $K = 8$ may originate in an interaction with $K = 6$ of $v_8 = 4^{+2}$ directly or through q_{22} interaction with $K = 6$ of $v_4 = v_8 = 1^{-1}$ as judged from the energy level diagram in Ref. [6]. The residuals in $K = 9$ are below 1 MHz for $J'' = 9$ and 13–18; assignments for $J'' = 60$ and 61 are tentative; the magnitudes of the residuals are slightly larger for these two transitions. Assignments for $K = 10$ cover $J'' = 13$ to 18 and 60 and 61. The measured frequencies are between 18 and 26 MHz lower than the calculated ones. A likely explanation is a perturbation with $K = 11$ of $v_7 = 1^{-1}$, which is ~1 cm^{-1} higher at low J, increasing at higher J. The assignment of $J'' = 61$ in $K = 11$ to a line close to the calculated position is very tentative.

Transitions in $v_4 = v_8 = 1^{-1}$ extend to $K = 8$, and the coverage is good up to $K = 5$. There appear to be no perturbations in $K = 0$, and residuals in $K = 1$ to 3 are below 1.5 MHz. $K = 4$

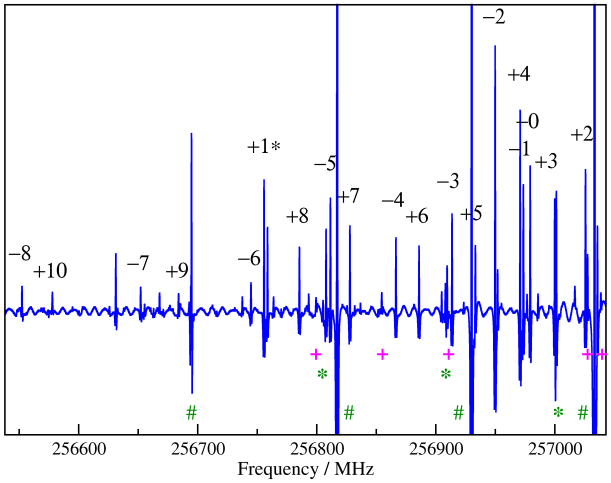

Figure 9: Detail of the millimeter spectrum of CH_3CN in the region of the $J = 14-13$ transition of $v_4 = v_8 = 1$. The $k = K \times l$ quantum numbers are given for this state. The lower frequency transition with $k = +1$ is marked with an asterisk; the higher frequency transition is more than 200 MHz higher than the $k = +2$ line. Assigned, sufficiently strong transitions are marked by a pound and plus signs below the zero level for $v = 0$ and $v_7 = 1$ of CH_3CN, respectively, asterisks below the zero level indicate transitions of $v = 0$ of $CH_3{}^{13}CN$.

Table 8: Spectroscopic parameters X or differences $\Delta\Delta X$ thereof [a,b] (cm^{-1}, MHz)[c] of methyl cyanide in its $v_4 = v_8 = 1$ state.

Parameter X	Value
$E_{\rm vib}$ [c]	1290.052130 (12)
$\Delta\Delta(A-B)$	−26.44 (4)
$\Delta\Delta B$	−0.13917 (11)
$\Delta\Delta D_{JK} \times 10^3$	2.582 (16)
$\Delta\Delta D_J \times 10^6$	−25.69 (6)
$\Delta\Delta H_{KJ} \times 10^6$	29.8 (7)
$\Delta\Delta H_{JK} \times 10^9$	−97.0 (14)
$\Delta\Delta H_J \times 10^{12}$	86.6 (98)
$\Delta\Delta A\zeta$	−21.93 (6)
$\Delta\Delta\eta_J \times 10^3$	25.58 (9)
$\Delta\Delta\eta_{JK} \times 10^6$	−106. (5)
$\Delta\Delta q$	−0.23155 (20)
$\Delta\Delta q_J \times 10^6$	−14.98 (16)
$\Delta\Delta q_{JJ} \times 10^{12}$	−348. (27)

[a] Numbers in parentheses are one standard deviation in units of the least significant figures. See Ref. [2] for sign and value considerations.

[b] Parameter difference $\Delta\Delta X = X - \Delta X_4 - \Delta X_8$; $\Delta X_4 := 0$ if X_4 is not defined.

[c] All parameters given in units of megahertz, except for $E_{\rm vib}$, which is given in units of inverse centimeters.

is also only slightly perturbed for $J'' \leq 33$, less than 1.3 MHz. However, five transitions with $43 \leq J'' \leq 63$ display rapidly increasing residuals from more than 6 MHz to ∼162 MHz. An interaction with $K = 2$ of $v_3 = 1$ is a probable explanation. This interaction is in the model of Ref. [5]. The anharmonic resonances with $v_7 = v_8 = 1^{+2}$ and $v_8 = 4^{+2}$ mentioned earlier in this section may cause the small deviations in $K = 5$ and slightly larger ones in $K = 6$ of $v_4 = v_8 = 1^{-1}$. Transitions with $J'' = 9$ and 13−18 were assigned quite confidently for $K = 6$. The assignment of a somewhat more perturbed line to $J'' = 61$ is tentative. Residuals in $K = 7$ increase in magnitude from −8.5 MHz to −15.9 MHz at $J'' = 9$ and 13−18 and decrease somewhat for $J'' = 60$ and 61. The residuals in $K = 8$ are larger, increasing in magnitude from −16.9 MHz to −34.4 MHz at $J'' = 9$ and 13−18. The model in Ref. [6] includes a $\Delta K = -1$, $\Delta l = +2$ interaction with $v_6 = 1^{+1}$, which may be responsible for the perturbations.

Perturbed rotational transitions were weighted out by adding sufficiently large megahertz values to the uncertainties that they do not contribute adversely to the rms error. The resulting vibrational energy and the spectroscopic parameters $\Delta\Delta X$ are given in **Table 8**. There are 267 rotational transitions with 256 different frequencies not weighted out with an rms error of 0.984 and an rms of 58.4 kHz. As usual in line lists with greatly varying uncertainties, the rms is dominated by the data with relatively large residuals. The 626 IR transitions (562 different frequencies) with 0.0002 cm^{-1} uncertainty and the 120 IR transitions (111 different frequencies) with mostly 0.0004 cm^{-1} uncertainty display rms values of 0.00016 and 0.00034 cm^{-1}, respectively, possibly judged somewhat conservatively considering that deperturbations may improve the rms values. The line, parameter, and fit files are available as supplementary material. Additional files will also provided in the CDMS, as in the case of the global fit up to $v_4 = 1$.

4. Astronomical results

We use the spectroscopic results obtained in Sect. 3 to investigate the methyl cyanide emission toward the main hot molecular core of the Sgr B2(N) star-forming region. We employ data acquired in the course of the imaging spectral line survey ReMoCA carried out toward Sgr B2(N) with ALMA in the 3 mm atmospheric window. A detailed description of the observations and data analysis was reported in [31]. In short, the survey was performed with five different frequency tunings, which we call Setups 1 to 5 (S1–S5), covering the full frequency range from 84.1 to 114.4 GHz with a spectral resolution of 488 kHz that corresponds to a velocity resolution of 1.7 to 1.3 km s^{-1}. The phase center of the interferometric observations was set at $(\alpha, \delta)_{\rm J2000}$= ($17^{\rm h}47^{\rm m}19.87^{\rm s}$, $-28°22'16.0''$). This position is located half-way between the hot cores Sgr B2(N1) and Sgr B2(N2) which are separated by 4.9″ or ∼0.2 pc at the distance of Sgr B2 (∼8.2 kpc, [64]). Following the same strategy as in [31], we analyzed the spectrum at the offset position Sgr B2(N1S) at which the optical depth of the continuum emission is lower than toward the peak of Sgr B2(N1), where it is partially optically thick, obscuring the molecular line

emission arising from compact regions. This offset position is located at $(\alpha, \delta)_{J2000}$= ($17^h47^m19.870^s$, $-28°22'19.48''$), about $1''$ to the south of Sgr B2(N1). Depending on the Setup, the angular resolution (HPBW) varies between ∼0.3″ and ∼0.8″, with a median value of 0.6″. The rms sensitivity ranges from 0.35 mJy beam^{-1} to 1.1 mJy beam^{-1}, with a median value of 0.8 mJy beam^{-1}. The continuum and line contributions were separated as described in [31], with an improvement performed later as reported in [65].

The density of the gas probed in emission with ReMoCA toward Sgr B2(N)'s hot cores is higher than 10^7 cm^{-3} ([66]) which allows us to assume local thermodynamic equilibrium (LTE) to produce synthetic spectra of complex organic species such as methyl cyanide. For this, we used the Weeds software ([67]). We modeled each identified species with a set of five parameters: size of the emitting region (θ_s), column density (N), temperature (T_{rot}), linewidth (ΔV), and velocity offset (V_{off}) with respect to the assumed systemic velocity of the source (V_{sys} = 62 km s^{-1}). We derived a best-fit model for each species and added the contributions of all identified species together.

We followed this strategy to model the rotational emission of methyl cyanide, its singly-substituted ^{13}C and ^{15}N isotopologs, and its doubly-substituted ^{13}C isotopolog toward Sgr B2(N1S). Apart from the predictions obtained in this work for CH_3CN $v_4 = 1$ and $v_4 = v_8 = 1$, we used the spectroscopic predictions available in the Cologne Database for Molecular Spectroscopy (CDMS, [46]), more precisely version 2 of the entry with hyperfine structure 41505 for CH_3CN $v = 0$, version 1 of the entries with hyperfine structure 41509 for CH_3CN $v_8 = 1$, 41510 for CH_3CN $v_8 = 2$, 42508 for $^{13}CH_3CN$ $v = 0$, 42513 for $^{13}CH_3CN$ $v_8 = 1$, 42509 for $CH_3{}^{13}CN$ $v = 0$, 42514 for $CH_3{}^{13}CN$ $v_8 = 1$, 43513 for $^{13}CH_3{}^{13}CN$ $v = 0$, and version 1 of the entries 42510 for $CH_3C^{15}N$ $v = 0$ and 42515 for $CH_3C^{15}N$ $v_8 = 1$. The CH_3CN entries with $v_8 \leq 2$ are based on Ref. [2] with considerable ground state contributions, also in the range of our study, from Ref. [59]. The isotopic ground state entries are based on [27] with data from that study and in part from previous reports; $CH_3{}^{13}CN$ and $^{13}CH_3CN$ transitions in the range of our study were taken from Ref. [68]; transitions of $CH_3C^{15}N$ from Ref. [69]. The isotopic entries involving $v_8 = 1$ are based on [28]; the lower frequency data of $CH_3C^{15}N$, encompassing the range of our survey, are from Ref. [55].

The best-fit spectra obtained for the various vibrational states of methyl cyanide and its isotopologs are shown in **Figs. 10**, **11**, and **B.12–B.21**. These spectra were obtained in the following way. On the basis of our complete model that includes all molecules identified in the spectrum of Sgr B2(N1S) so far, we selected the transitions of methyl cyanide and its isotopologs that are not significantly contaminated by the emission of other species. We produced integrated intensity maps of these transitions to measure the size of the methyl cyanide emission. These maps are shown in **Figs. B.22–B.24**, and the sizes derived from two-dimensional Gaussian fits to these maps are plotted in **Figs. B.25–B.27**. We see a clear dependence of the emission size with the upper-level energy of the transitions, varying from ∼2.5″ at low energy to ∼1.5″ at high energy, which is still at least a factor two larger than the angular resolution of the ReMoCA survey. A similar behavior is also seen for methanol in the same data set (see Fig. 4 of [70]). To produce the synthetic spectra of methyl cyanide and its isotopologs, we assumed an emission size of 1.6″, close to the emission size of the high-energy transitions.

Table 9: Rotational temperatures derived from population diagrams toward Sgr B2(N1S).

Molecule	States[a]	T_{fit}[b] (K)
CH_3CN	$v_8 = 1$, $v_8 = 2$, $v_4 = 1$, $v_4 = v_8 = 1$	296 (14)
$^{13}CH_3CN$	$v = 0$, $v_8 = 1$	341 (70)
$CH_3{}^{13}CN$	$v = 0$, $v_8 = 1$	350 (36)

[a] Vibrational states that were taken into account to fit the population diagram. [b] The standard deviation of the fit is given in parentheses. As explained in Sect. 4.4 of [31], this uncertainty is purely statistical and should be viewed with caution. It may be underestimated.

We selected the transitions of methyl cyanide and its isotopologs that are not too much contaminated by emission from other species and that have a peak optical depth lower than 2.5 to produce population diagrams. Following the strategy of [3], we corrected these diagrams for the line optical depths and contamination from other species. These population diagrams are shown in **Figs. B.28–B.30**. A fit to these diagrams yields an estimate of the rotational temperature. The fit results are listed in **Table 9**. We obtain rotational temperatures on the order of 300 K. However, as explained in [3] and [31], these estimates are affected by several systematic uncertainties such as the varying level of continuum emission and, more importantly, the residual contamination of still unidentified species. In addition, our simple Weeds modeling procedure, that assumes a uniform emission, cannot account for density and temperature gradients along the line of sight. Optically thick lines trace more external layers of the hot core which have lower gas temperatures, hence they saturate at lower intensities compared to the synthetic spectra. This is particularly obvious for the highly optically thick $v = 0$ lines of CH_3CN shown in **Fig. B.12**, but it also affects the lower-energy lines of $v_8 = 1$ and $v_8 = 2$ of CH_3CN as well as $v = 0$ of the singly-substituted ^{13}C isotopologs. These optically thick lines at low energy, tracing colder material and thus being weaker, bias the fits of the population diagrams toward higher temperatures. To produce the synthetic spectra, we decided to use a lower temperature of 260 K. The LTE parameters of the best-fit models are listed in **Table 10**. Another constraint that we took into account to obtain the best-fit model is the $^{12}C/^{13}C$ isotopic ratio that is known to be in the range 20–25 for a number of complex organic molecules in Sgr B2(N) (see, e.g., [71], [3], [72]).

On the basis of the best-fit synthetic spectra obtained above, we get a clear detection of methyl cyanide transitions from within $v_4 = 1$ toward Sgr B2(N1S) (**Fig. 10**). Because of blends with other species, the detection of $v_4 = v_8 = 1$ is more tentative, but the excellent agreement we obtain between the synthetic and observed spectra at 91784 MHz gives us confidence

Table 10: Parameters of our best-fit LTE model of methyl cyanide toward Sgr B2(N1S).

Molecule	Status[a]	N_{det}[b]	θ_s[c] ($''$)	T_{rot}[d] (K)	N[e] (cm^{-2})	F_{vib}[f]	ΔV[g] (km s^{-1})	V_{off}[h] (km s^{-1})	$\frac{N_{ref}}{N}$[i]
CH_3CN, $v = 0^\star$	d	9	1.6	260	2.8 (18)	1.00	6.0	−0.2	1
$v_8 = 1$	d	22	1.6	260	2.8 (18)	1.00	6.0	−0.2	1
$v_8 = 2$	d	16	1.6	260	2.8 (18)	1.00	6.0	−0.2	1
$v_4 = 1$	d	4	1.6	260	2.8 (18)	1.00	6.0	−0.2	1
$v_4 = v_8 = 1$	t	1	1.6	260	2.8 (18)	1.00	6.0	−0.2	1
$^{13}CH_3CN$, $v = 0$	d	9	1.6	260	1.4 (17)	1.35	6.0	−0.2	21
$v_8 = 1$	d	4	1.6	260	1.4 (17)	1.35	6.0	−0.2	21
$CH_3{}^{13}CN$, $v = 0$	d	6	1.6	260	1.4 (17)	1.35	6.0	−0.2	21
$v_8 = 1$	d	10	1.6	260	1.4 (17)	1.35	6.0	−0.2	21
$^{13}CH_3{}^{13}CN$, $v = 0$	t	1	1.6	260	6.8 (15)	1.35	6.0	−0.2	415
$CH_3C^{15}N$, $v = 0$	n	0	1.6	260	< 1.4 (16)	1.35	6.0	−0.2	> 207
$v_8 = 1$	n	0	1.6	260	< 1.4 (16)	1.35	6.0	−0.2	> 207

[a] d: detection, t: tentative detection, n: nondetection. [b] Number of detected lines (conservative estimate, see Sect. 3 of [3]). One line of a given species may mean a group of transitions of that species that are blended together. [c] Source diameter (*FWHM*). [d] Rotational temperature. [e] Total column density of the molecule. x (y) means $x \times 10^y$. An identical value for all listed vibrational states of a molecule means that LTE is an adequate description of the vibrational excitation. [f] Correction factor that was applied to the column density to account for the contribution of vibrationally excited states, in the cases where this contribution was not included in the partition function of the spectroscopic predictions. [g] Linewidth (*FWHM*). [h] Velocity offset with respect to the assumed systemic velocity of Sgr B2(N1S), V_{sys} = 62 km s^{-1}. [i] Column density ratio, with N_{ref} the column density of the previous reference species marked with a ⋆.

in the identification of this state in the ReMoCA data **(Fig. 11)**.

The doubly-substituted ^{13}C isotopolog of methyl cyanide is only tentatively detected, on the basis of one line at 107106 MHz which is partly contaminated by emission from CH_3COOH $v_t = 1$ (**Fig. B.19**). The synthetic spectra that we obtained for $CH_3C^{15}N$ $v = 0$ and $v_8 = 1$ are consistent with the observed spectra, but there are too many blends with other species to claim a detection. The column density listed in **Table 10** for this isotopolog should rather be seen as an upper limit.

5. Discussion of spectroscopic results

Our model of low-lying vibrational states of CH_3CN up to $v_8 = 2$ [2] was extended to include $v_4 = 1$. Additional or improved data were obtained in particular for $v_8 = 2$. The ground state spectroscopic parameter values and uncertainties in **Table 4** were largely unaffected, at least with respect to the uncertainties. Notable exceptions are the purely axial parameters $A - B$, D_K, and H_K, whose uncertainties were lowered mostly by the $v_4 = 1$ resonances with $v_8 = 2$ and 3. Their values, however, appear to change too much as the rms error of the $\Delta K = 3$ ground state combination loops roughly doubles to about 1.3, see **Table 2**, a value that is somewhat too high for a fully satisfactory fit. Possible explanations may be unaccounted perturbations in the present data set or a too optimistic judgment of the $\Delta K = 3$ ground state combination loops [30]. Unsurprisingly, the rms and the rms error hardly changed for the $v = 0$ and $v_8 = 1$ rotational data and the ν_8 data with respect to our previous study [2]. Small to moderate changes occured for the $v_8 = 2$ rotational and rovibrational data. The present ν_4 data fit to 0.00009 cm^{-1}, compared with 0.00013 cm^{-1} previously [5]. Part of the somewhat large rms error of the $v_4 = 1$ rotational data is caused by residuals from transitions involving $J = 56$ and $K = 7$, pointing at the need to improve the treatment of the interaction with $v_8 = 3^{-1}$.

The $v_4 = 1$ parameters from the present investigation and those from the previous study [5] are in a complex relationship, as can be seen in **Table 4**. First, the extensive amount of rotational data in the present analysis required many more spectroscopic parameters, up to tenth order. E_{vib}, ΔB, ΔD_{JK}, and ΔD_J are quite similar. The values of $\Delta(A - B)$, ΔD_K, and in particular ΔH_K differ considerably with respect to the uncertainties. The value previously employed for H_K in the ground vibrational state, ~156 Hz [5], is identical to our present value, therefore not suited to explain the difference. One explanation may be that our IR data extend to $K = 13$, whereas those in Ref. [5] extend only to $K = 12$. While this is not a large difference, it may be enough to explain the differences in ΔH_K, especially taking into account the relatively large uncertainties, and the concomitant changes in $\Delta(A - B)$ and ΔD_K. Another explanation may be associated with the differences in observed and treated perturbations.

The magnitudes of ΔX compared to those of the ground state X are noteworthy for the parameters of sixth order and higher in our present parameter set. The magnitudes of ΔX are much larger in particular for the highly K dependent parameters ΔH_{KJ}, ΔL_{KKJ}, and ΔP_{KKJ}, and all these vibrational changes are negative. This could be an indication of a perturbation. However, there is no indication of a correspondence in the $v_8 = 2^0$ parameters caused by a purported strong Fermi resonance [15]. In addition, trial fits with various values of $F(4, 8^{2,0})$ did not affect more than one or two of the ΔX substantially. Literature values do not provide evidence that these peculiar parameter

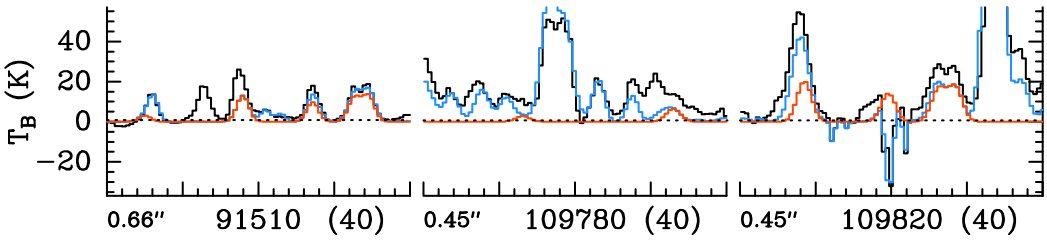

Figure 10: Transitions of CH_3CN, $v_4 = 1$ covered by our ALMA survey. The best-fit LTE synthetic spectrum of CH_3CN, $v_4 = 1$ is displayed in red and overlaid on the observed spectrum of Sgr B2(N1S) shown in black. The blue synthetic spectrum contains the contributions of all molecules identified in our survey so far, including the species shown in red. The central frequency and width (in parenthesis) are indicated in MHz below each panel. The angular resolution (HPBW) is also indicated. The y-axis is labeled in brightness temperature units (K). The dotted line indicates the 3σ noise level.

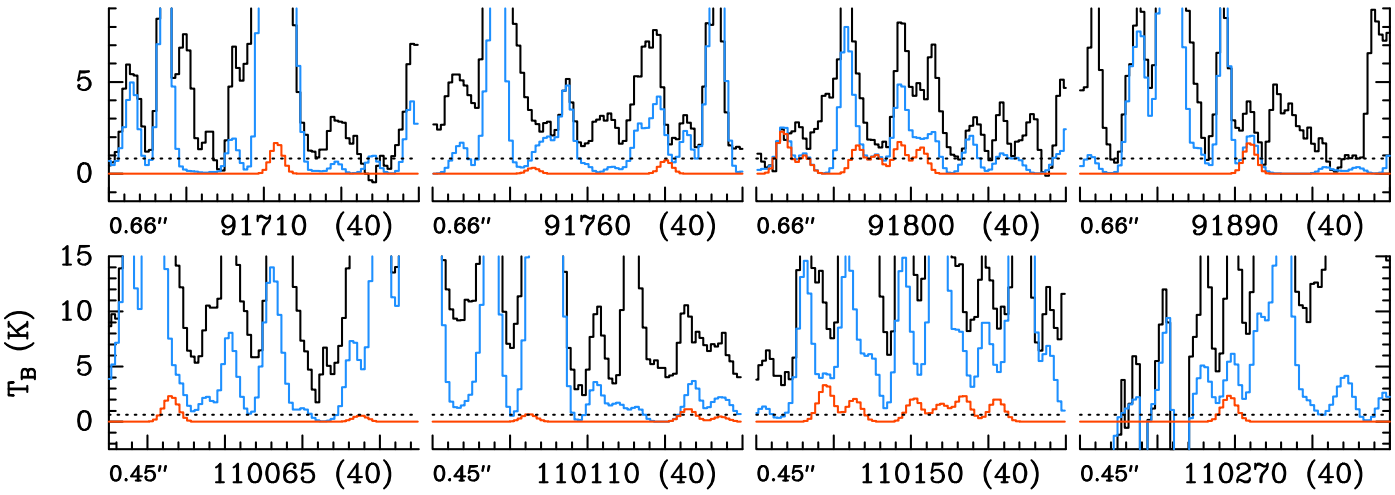

Figure 11: Same as Fig. 10 but for CH_3CN, $v_4 = v_8 = 1$.

values may be caused by Coriolis interaction with $v_7 = 1$ or $v_6 = 1$. The ΔH_{KJ} value in Ref. [5] is similar in value to ours, and their IR and rotational data extend to $K = 12$. In contrast, their data in ν_7 and the ν_6 data in Ref. [6] extend to $K = 15$, and ΔH_{KJ} was constrained to zero for either vibrational state. Trial fits with $G_b(4, 7)$ increased pointed in the same direction. It may thus be that these vibrational changes are intrinsic to this vibrational mode which is the stretching mode of a long and fairly weak C−C single bond.

Our integrated band strength of ν_4 agrees well with previously reported values from low- or medium-resolution spectroscopic studies, as summarized in **Table 3**; the agreement is slightly worse for $2\nu_8$ and more so for ν_8, possibly reflecting the challenges of far-IR measurements.

Some $v_8 = 3$ parameters in **Table 5** differ with respect to the entirely fixed values used in our previous study. The value of $A\zeta$ in $v_8 = 3^3$ is expected to be closer to the value presently assumed than the one from Ref. [5], as can be seen by comparison with the $v_8 = 1$ and 2 values in **Table 7**. Our $3\nu_8^3$ origin of 1122.35 cm^{-1} is only slightly different from 1122.15 cm^{-1} in Ref. [5] and in very good agreement with the extrapolated value of 1122.34 cm^{-1} in Ref. [5]. In addition, our $v_8 = 3$ $\Delta(A - B)$ value of -442.06 ± 0.06 MHz agrees quite well with the extrapolated -459.6 ± 4.5 MHz derived from Ref. [5]. This demonstrates that the rotational transitions in $v_4 = 1$ contain information on the band origins of $v_8 = 3^3$ and 3^1 through perturbations between $v_8 = 3$ and $v_4 = 1$, notably the proximity of $J = 42$ of $K = 7$ in $v_4 = 1$ and $K = 1$ in $v_8 = 3^{-3}$. An improved treatment of the $v_8 = 3$ interactions with $v_8 = 2$ and $v_4 = 1$ requires $v_8 = 3$ and $v_7 = 1$ data to be added to the line list. The $v_7 = 1$ data are necessary because of the widespread interaction between $v_7 = 1$ and $v_8 = 3$. The $v_8 = 3$ and $v_7 = 1$ data need to be added with caution because both states are perturbed by higher lying states such as $v_4 = v_8 = 1$ or $v_8 = 4$. A more firm determination of the purely axial $v_8 = 3^3$ parameters may necessitate assignments in $3\nu_8^3 - 2\nu_8^2$ because $3\nu_8^3 - \nu_8^1$ is forbidden to first order and acquires intensity only through q_{22} interaction with the strongly allowed $3\nu_8^1 - \nu_8^1$ hot band.

Several of the interaction parameters in **Table 6** have now smaller uncertainties; F_2 of the $v_8 = 1$ and 2 interaction is an exception because of $F_{2,J}$ in the present fit. The $v_8 = 2$ and 3 Fermi parameters not only have smaller uncertainties, but $F(8^{2,\pm2}, 8^{3,\mp1}) \approx 75967$ MHz is much closer to the theoretical $\sqrt{2} \times F(8^{\pm1}, 8^{2,\mp2}) = 75148$ MHz than ~77208 MHz from our previous work [2]. The value 90876 MHz of $F(8^{2,0}, 8^{3,3})$, on the other hand, differs slightly more from $\sqrt{3} \times F(8^{\pm1}, 8^{2,\mp2})$ or 92037 MHz, see also, e.g., Ref. [9]. Such deviations are common if a resonance is approached only from one side and for one of the interacting (sub-) states. Since the final interaction parameter values should be closer to the ideal values, we tried a fit constraining these parameters to the ideal ratios with $F(8^{\pm1}, 8^{2,\mp2})$. The rms error of the fit deteriorated moderately from 0.853 to 0.914, but the largest part of this was caused by a deterioration of the $v_8 = 2^0$ rotational data from 0.965 to 1.403, which is not surprising, given that the current $F(8^{2,0}, 8^{3,3})$ value deviated much more from the ideal ratio than $F(8^{2,\pm2}, 8^{3,\mp1})$. All attempts to improve the quality of the fit were unsatisfactory, and we discarded this fit. Possible explanations for the deterioration may be, for example, unfavorable $v_8 = 3$ parameters or the truncation of the Hamiltonian at $v_8 = 3$. The values describing the resonances between $v_4 = 1$ and $v_8 = 3$ look quite reasonable, but the number and choice of parameters as well as their values may change when extensive $v_8 = 3$ data will have been added to the line list or when truncation of the Hamiltonian, in particular in v_8, is less of an issue.

The $v_8 = 1$ and 2 parameters in **Table 7** display some changes in values and uncertainties which are caused in complex and different ways by introducing several constraints, additional transition frequencies for these states, and further energy constraints through the interactions of $v_4 = 1$ with $v_8 = 2$ and 3. The changes are most pronounced in $E_{\rm vib}$, $\Delta(A - B)$, ΔD_K, and in the one ΔH_K used for $v_8 = 1$. Trial fits with the two $v_8 = 2$ ΔH_K values constrained to two times the $v_8 = 1$ value increased the rms error of the entire fit and of the $\Delta K = 3$ ground state combination loops somewhat more, therefore, these constraints were omitted for now.

A set of spectroscopic parameters of $v_4 = v_8 = 1$ was determined. The vibrational changes are often not particularly small, but this may be caused, at least in part, by not treating any of the perturbations. One of the important states in this regard is $v_8 = 4$, whose estimation of spectroscopic parameters will likely benefit from improved $v_8 = 3$ parameters. It will be very important that these estimates are very good in order to be able to account properly for the perturbations in the $v_4 = v_8 = 1$ rotational data because of the strong $\Delta K = \pm2$, $\Delta l = \pm2$ interactions and possibly $\Delta K = \pm4$, $\Delta l = \pm4$ interactions. We point out that interacrtions up to $\Delta K = \pm8$, $\Delta l = \pm8$ are allowed in $v_8 = 4$.

Quantum-chemical calculations may be useful to disentangle the plethora of perturbations in low-lying vibrational states of CH_3CN. To the best of our knowledge, there are no published results available on, e.g., interaction parameters. However, numerous calculations are available on calculations of the anharmonic vibrations of CH_3CN, e.g. Refs. [73, 74, 75]. A very sensitive probe into the quality of such calculations is the energy splitting of the l components of $v_8 = n$. Presently available experimental numbers are summarized in **Table 11**. The splitting is determined to first order by $g_{ll}l^2$; a value of $g_{ll} = 5.6$ cm^{-1} accounts well for the experimental CH_3CN values in Table 11.

Even though the $v_8 = 4$ values were estimated, there is little doubt on the origin of $v_8 = 4^4$; its value can be evaluated from various information available for CH_3CN and $CH_3C^{15}N$. Combining the origin of $4\nu_8^4 - \nu_8$ of $CH_3C^{15}N$, 1140.626±0.032 cm^{-1} [25], with the estimate of the ν_8 band origin, 362.41 cm^{-1} [28, 15], yields 1503.04 cm^{-1} as estimate of the $4\nu_8^4$ band origin. This value may be scaled with the $^{14}N/^{15}N$ ratios of the ν_8 [28], $3\nu_8^3$ [18, 5], and $4\nu_8^2$ band origins [25, 28, 6] to arrive at an estimate for the $4\nu_8^4$ band origin of CH_3CN. The respective values are 1513.9, 1514.6, and 1514.3 cm^{-1}, in excellent agreement with our estimate of ~1514 cm^{-1} [2], see also **Table 1**.

Experimental values of the related molecules propyne and methyl isocyanide in **Table 11** are in line with those of methyl cyanide as far as they are available. In contrast, quantum-chemically derived values of CH_3CN agree poorly with the

Table 11: Experimental vibrational energy $E_{\rm vib}$ of $v_8 = 1$ of CH_3CN (cm^{-1}) and splitting $\Delta_{n,l1-l2}$ (cm^{-1}) of the l components of $v_8 = n$ in comparison to experimental values of related molecules and in comparison to quantum-chemical calculations.

	Experiment			Quantum-chemistry	
	CH_3CN^a	CH_3CCH^b	CH_3NC^c	CH_3CN^d	CH_3CN^e
$E_{\rm vib}$	365.0	330.9	267.3	364	360.991
$\Delta_{2,2-0}$	22.397	20.416	20.662	6	−0.646
$\Delta_{3,3-1}$	44.56	40.872		7	−1.222
$\Delta_{4,2-0}$	22				−0.576
$\Delta_{4,4-2}$	66				−1.726

[a] Ref. [2] and this work.

[b] Refs. [8] and [9]; except $v_b = 3$ data from Ref. [10].

[c] Ref. [11].

[d] Ref. [73].

[e] Ref. [74].

experimental ones. The authors of Ref. [73] did not discuss their poor value for $v_8 = 2$ and alleged that the experimental $v_8 = 3$ value must be incorrect because the band centers were only "estimated experimental transitions". The $v_8 = 3^1$ origin, however, was determined directly through assignments in the perturbation allowed $3\nu_8^1$ band and through the fully allowed $3\nu_8^1 - \nu_8^1$ band [5]. The $v_8 = 3^3$ origin was derived through perturbations, but its value is quite close to the extrapolated one of 1122.339 cm^{-1}; our origin is actually still closer to this value. Assignments in the $3\nu_8^3 - 2\nu_8^2$ hot band would yield this origin directly, along with a value for $\Delta(A - B)$ (or ΔA). Our $v_8 = 3^1$ origin is quite precise, however, it depends somewhat on the $\Delta(A-B)$ value used in the fit which is marginally smaller in magnitude than the extrapolated value derived from ΔA in Ref [5]. The data in Ref. [74] are somewhat better represented by one g_{ll} value of about −0.6 cm^{-1}, but additional correction would be needed for quantitative agreement. In addition, the values disagree in sign and in magnitude and disagree more with the experimental values than those from Ref. [74]. There is only one value for $\Delta_{2,2-0} = 0.925$ cm^{-1} in Ref. [74]. In order to be helpful for disentangling the perturbations in low-lying states of methyl cyanide, it is necessary that future quantum-chemical calculations reduce these deviations substantially.

6. Conclusions and outlook

Data of $v_4 = 1$ have been added to our model of low-lying vibrational states of CH_3CN up to $v_8 = 2$ [2]. The analysis revealed new rovibrational interactions and improved several interactions treated already earlier. One important outcome is that now all four l-components of $v_8 = 3$ are linked in energy to $v_4 = 1$. The analysis of interacting states of methyl cyanide up to $v_4 = 1$ has probably been developed to the extent that is possible without inclusion of extensive $v_7 = 1$ and $v_8 = 3$ data. Earlier, perturbations in $v_4 = 1$ that were not treated likely caused the problems we encountered in adding this state to our global model. Adding $v_7 = 1$ and $v_8 = 3$ data needs to be done with caution because these two states are not only perturbed by each other and the lower lying states $v_4 = 1$ and $v_8 = 2$, but also by higher lying states such as $v_4 = v_8 = 1$ or $v_8 = 4$, among others. Our earlier problems with including $v_7 = 1$ and $v_8 = 3$ probably arose from underestimating the amount of perturbations in these states. Recently, spectra in the region of ν_8 of CH_3CN were recorded at the Canadian Light Source. These may be very beneficial for the analyses of $v_8 = 3$ and possibly even $v_8 = 4$. Not only transitions of the ν_8 cold band were easily identified, but also some of the $2\nu_8 - \nu_8$ hot band. The $3\nu_8 - 2\nu_8$ hot band should also be identifiable, potentially even $4\nu_8-3\nu_8$. Rotational transitions up to $v_8 = 4$ have sufficient intensity at room temperature to study them quite extensively. Investigations of states up to $v_8 = 5$ should be possible, but this may be challenging.

Assignments in $\nu_4 + \nu_8 - \nu_8$ and in $v_4 = v_8 = 1$ were made, and a simple model was developed to account for a fair fraction of these data. This model should be useful for the upcoming reanalysis of $v_7 = 1$ and $v_8 = 3$ data even if the $v_4 = v_8 = 1$ data and their perturbations will be left untouched because of the plethora of interactions with higher lying states.

Rotational transitions of methyl cyanide from within all vibrational states up to $v_4 = 1$ were detected with ALMA in the hot molecular core of Sgr B2(N1). The tentative detection of $v_4 = v_8 = 1$ bodes well for the future detection of the slightly lower-energy vibrational states $v_7 = 1$ and $v_8 = 3$.

Acknowledgements

It is our pleasure to dedicate this article to Stephan Schlemmer. We thank the reviewers for their questions and suggestions which helped to clarify some aspects of the manuscript. We thank Robert L. Sams for recording the ν_4 infrared spectrum, Isabelle Kleiner for initial assignments and early modeling efforts, and Linda R. Brown for the final calibration of the IR spectrum, the generation of a peak list, and further initial assignments in $\nu_4 + \nu_8 - \nu_8$. We also thank John C. Pearson for recording part of the submillimeter spectra at JPL. We are grateful for support by the Deutsche Forschungsgemeinschaft (DFG) via the collaborative research center SFB 956 (project ID 184018867), sub-project B3. The portion of this work which was carried out at the Jet Propulsion Laboratory, California Institute of Technology was performed under contract with the National Aeronautics and Space Administration. The infrared spectrum analyzed in the present study was recorded at the W.R. Wiley Environmental Molecular Sciences Laboratory, a national scientific user facility sponsored by the Department of Energy's Office of Biological and Environmental Research located at the Pacific Northwest National Laboratory (PNNL). PNNL is operated for the United States Department of Energy by the Battelle Memorial Institute under Contract DE-AC05-76RLO1830. Our research benefited from NASA's Astrophysics Data System (ADS).

Appendix A. Supplementary Material

The following are the Supplementary data to this article: The parameter, line, and fit files of the global fit (16u4.∗) and of the isolated fit (4plus8QN.∗) along with a readme file are provided.

Appendix B. Additional Figures

Figures B.12–B.21 show spectra of the transitions of CH_3CN $v = 0$, $v_8 = 1$, $v_8 = 2$, $^{13}CH_3CN$ $v = 0$, $v_8 = 1$, $CH_3{}^{13}CN$ $v = 0$, $v_8 = 1$, $^{13}CH_3{}^{13}CN$ $v = 0$, and $CH_3C^{15}N$ $v = 0$, $v_8 = 1$, respectively, covered by the ReMoCA survey of Sgr B2(N1S) performed with ALMA. Figures B.22–B.24 show integrated intensity maps of uncontaminated transitions of CH_3CN, $^{13}CH_3CN$, and $CH_3{}^{13}CN$, respectively. Figures B.25–B.27 show the emission sizes of CH_3CN, $^{13}CH_3CN$, and $CH_3{}^{13}CN$, respectively, as derived from two-dimensional Gaussian fits to these maps. Figures B.28–B.30 show population diagrams of CH_3CN, $^{13}CH_3CN$, and $CH_3{}^{13}CN$, respectively.

References

[1] P. M. Solomon, K. B. Jefferts, A. A. Penzias, R. W. Wilson, Detection of Millimeter Emission Lines from Interstellar Methyl Cyanide, Astrophys. J. Lett. 168 (1971) L107–L110. doi:10.1086/180794.

[2] H. S. P. Müller, L. R. Brown, B. J. Drouin, J. C. Pearson, I. Kleiner, R. L. Sams, K. Sung, M. H. Ordu, F. Lewen, Rotational spectroscopy as a tool to investigate interactions between vibrational polyads in symmetric top molecules: Low-lying states $v_8 \leq 2$ of methyl cyanide, CH_3CN, J. Mol. Spectrosc. 312 (2015) 22–37. arXiv:1502.06867, doi:10.1016/j.jms.2015.02.009.

[3] A. Belloche, H. S. P. Müller, R. T. Garrod, K. M. Menten, Exploring molecular complexity with ALMA (EMoCA): Deuterated complex organic molecules in Sagittarius B2(N2), Astron. Astrophys. 587 (2016) A91. arXiv:1511.05721, doi:10.1051/0004-6361/201527268.

[4] H. Calcutt, J. K. Jørgensen, H. S. P. Müller, L. E. Kristensen, A. Coutens, T. L. Bourke, R. T. Garrod, M. V. Persson, M. H. D. van der Wiel, E. F. van Dishoeck, S. F. Wampfler, The ALMA-PILS survey: complex nitriles towards IRAS 16293-2422, Astron. Astrophys. 616 (2018) A90. arXiv:1804.09210, doi:10.1051/0004-6361/201732289.

[5] A. M. Tolonen, M. Koivusaari, R. Paso, J. Schroderus, S. Alanko, R. Anttila, The Infrared Spectrum of Methyl Cyanide Between 850 and 1150 cm^{-1}: Analysis of the ν_4, ν_7, and $3\nu_8^1$ Bands with Resonances, J. Mol. Spectrosc. 160 (2) (1993) 554–565. doi:10.1006/jmsp.1993.1201.

[6] R. Paso, R. Anttila, M. Koivusaari, The Infrared Spectrum of Methyl Cyanide Between 1240 and 1650 cm^{-1}: The Coupled Band System ν_3, $\nu_6^{\pm 1}$, and $(\nu_7 + \nu_8)^{\pm 2}$, J. Mol. Spectrosc. 165 (2) (1994) 470–480. doi:10.1006/jmsp.1994.1150.

[7] H. Ring, H. Edwards, M. Kessler, W. Gordy, Microwave Spectra: Methyl Cyanide and Methyl Isocyanide, Phys. Rev. 72 (12) (1947) 1262–1263. doi:10.1103/PhysRev.72.1262.2.

[8] H. S. P. Müller, P. Pracna, V. M. Horneman, The $v_{10} = 1$ Level of Propyne, $H_3C{-}C{\equiv}CH$, and Its Interactions with $v_9 = 1$ and $v_{10} = 2$, J. Mol. Spectrosc. 216 (2) (2002) 397–407. doi:10.1006/jmsp.2002.8661.

[9] P. Pracna, H. S. P. Müller, S. Klee, V. M. Horneman, Interactions in symmetric top molecules between vibrational polyads: rotational and rovibrational spectroscopy of low-lying states of propyne, $H_3C{-}C{\equiv}CH$, Mol. Phys. 102 (14) (2004) 1555–1568. doi:10.1080/00268970410001725864.

[10] P. Pracna, H. S. P. Müller, Š. Urban, V. M. Horneman, S. Klee, Interactions between vibrational polyads of propyne, $H_3C{-}C{\equiv}CH$: Rotational and rovibrational spectroscopy of the levels around 1000 cm^{-1}, J. Mol. Spectrosc. 256 (1) (2009) 152–162. doi:10.1016/j.jms.2009.04.003.

[11] P. Pracna, J. Urban, O. Votava, Z. Meltzerová, Š. Urban, V. M. Horneman, Rotational and rovibrational spectroscopy of the $v_8 = 1$ and 2 vibrational states of CH_3NC, Mol. Phys. 109 (17-18) (2011) 2237–2243. doi:10.1080/00268976.2011.605775.

[12] S. Kondo, W. B. Person, Infrared spectrum of acetonitrile: Analysis of Coriolis resonance, J. Mol. Spectrosc. 52 (2) (1974) 287–300. doi:10.1016/0022-2852(74)90120-9.

[13] A. Bauer, Interaction rotation-vibration dans le spectre de rotation des molécules d'acétonitrile $CH_3C^{14}N$ et $CH_3C^{15}N$, Ph.D. thesis, Université de Lille, Lille, France (1970).

[14] A. Bauer, M. Godon, Microwave spectra in the v_4 vibrational state of methyl cyanide and methyl isocyanide and their ^{15}N derivatives, Can. J. Phys. 53 (1975) 1154. doi:10.1139/p75-146.

[15] J. L. Duncan, D. C. McKean, F. Tullini, G. D. Nivellini, J. Perez Peña, Methyl cyanide. Spectroscopic studies of isotopically substituted species, and the harmonic potential function, J. Mol. Spectrosc. 69 (1) (1978) 123–140. doi:10.1016/0022-2852(78)90033-4.

[16] S. A. Rackley, R. J. Butcher, M. Römheld, S. M. Freund, T. Oka, Laser Stark spectroscopy of methyl cyanide in the 10-μm region: Analysis of the ν_4 and ν_7 bands, and the ν_7, $3\nu_8^1$ interaction, J. Mol. Spectrosc. 92 (1) (1982) 203–217. doi:10.1016/0022-2852(82)90094-7.

[17] Y. Mori, T. Nakagawa, K. Kuchitsu, Vibration-rotation spectra of CH_3CN: The ν_7 band and its hot bands near 1040 cm^{-1}, J. Mol. Spectrosc. 104 (2) (1984) 388–401. doi:10.1016/0022-2852(84)90132-2.

[18] A. Mito, J. Sakai, M. Katayama, Laser Stark spectroscopy of the ν_4 band of $CH_3C^{15}N$: Fermi resonance with $3\nu_8^3$, J. Mol. Spectrosc. 103 (1) (1984) 26–40. doi:10.1016/0022-2852(84)90143-7.

[19] P. Wallraff, K. M. T. Yamada, R. Schieder, G. Winnewisser, A digitally controlled diode-laser spectrometer: Infrared spectrum of the ν_4 band of acetonitrile between 890 and 960 cm^{-1}, J. Mol. Spectrosc. 112 (1) (1985) 163–172. doi:10.1016/0022-2852(85)90201-2.

[20] R. Bocquet, G. Wlodarczak, A. Bauer, J. Demaison, The submillimeter-wave rotational spectrum of methyl cyanide: Analysis of the ground and the low-lying excited vibrational states, J. Mol. Spectrosc. 127 (2) (1988) 382–389. doi:10.1016/0022-2852(88)90128-2.

[21] J. Cosleou, G. Wlodarczak, D. Boucher, J. Demaison, The rotational spectrum of CH_3CN in the $v_4 = 1$ state: Analysis of the Fermi resonance with $3\nu_8^3$, J. Mol. Spectrosc. 146 (1) (1991) 49–55. doi:10.1016/0022-2852(91)90369-L.

[22] H. Matsuura, Fermi Resonance with ν_6 of Acetonitrile, Bull. Chem. Soc. Japan 44 (9) (1971) 2379–2381. doi:10.1246/bcsj.44.2379.

[23] J. L. Duncan, D. Ellis, I. J. Wright, Analysis of the ν_3, ν_6, $\nu_7 + \nu_8$ Fermi and Coriolis interacting band system in methyl cyanide, Mol. Phys. 20 (4) (1971) 673–685. doi:10.1080/00268977100100641.

[24] H. Matsuura, N. Kubota, H. Murata, Vibration-Rotation Infrared Spectrum of ν_6 of Acetonitrile. Fermi and Coriolis Resonances with $\nu_7+\nu_8$ and ν_3, Chem. Lett. 11 (10) (1982) 1509–1512. doi:10.1246/cl.1982.1509.

[25] A. Mito, J. Sakai, M. Katayama, Laser stark spectroscopy of the $\nu_4 + \nu_8 - \nu_8$ band of $CH_3C^{15}N$: Fermi resonances with $4\nu_8^4$, $4\nu_8^2$, and $(\nu_7 + \nu_8)^2$, J. Mol. Spectrosc. 105 (2) (1984) 410–424. doi:10.1016/0022-2852(84)90230-3.

[26] C. P. Rinsland, V. Malathy Devi, D. C. Benner, T. A. Blake, R. L. Sams, L. R. Brown, I. Kleiner, A. Dehayem-Kamadjeu, H. S. P. Müller, R. R. Gamache, D. L. Niles, T. Masiello, Multispectrum analysis of the ν_4 band of CH_3CN: Positions, intensities, self- and N_2-broadening, and pressure-induced shifts, J. Quant. Spectrosc. Radiat. Transfer 109 (2008) 974–994. doi:10.1016/j.jqsrt.2007.11.013.

[27] H. S. P. Müller, B. J. Drouin, J. C. Pearson, Rotational spectra of isotopic species of methyl cyanide, CH_3CN, in their ground vibrational states up to terahertz frequencies, Astron. Astrophys. 506 (3) (2009) 1487–1499. arXiv:0910.3111, doi:10.1051/0004-6361/200912932.

[28] H. S. P. Müller, B. J. Drouin, J. C. Pearson, M. H. Ordu, N. Wehres, F. Lewen, Rotational spectra of isotopic species of methyl cyanide, CH_3CN, in their $v_8 = 1$ excited vibrational states, Astron. Astrophys. 586 (2016) A17. arXiv:1512.05271, doi:10.1051/0004-6361/201527602.

[29] H. S. P. Müller, B. J. Drouin, J. C. Pearson, L. R. Brown, I. Kleiner, R. L. Sams, Toward a Global Model of Low-Lying Vibrational States of CH_3CN: the $v_4 = 1$ State at 920 cm^{-1} and its Interactions with Nearby States, in: 65th International Symposium On Molecular Spectroscopy,

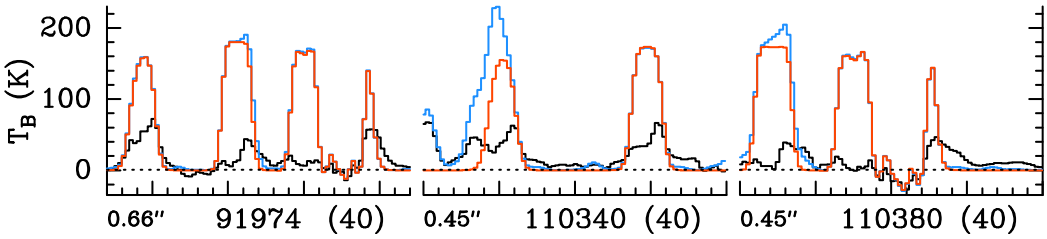

Figure B.12: Transitions of CH_3CN, $v = 0$ covered by our ALMA survey. The best-fit LTE synthetic spectrum of CH_3CN, $v = 0$ is displayed in red and overlaid on the observed spectrum of Sgr B2(N1S) shown in black. The blue synthetic spectrum contains the contributions of all molecules identified in our survey so far, including the species shown in red. The central frequency and width (in parenthesis) are indicated in MHz below each panel. The angular resolution (HPBW) is also indicated. The y-axis is labeled in brightness temperature units (K). The dotted line indicates the 3σ noise level.

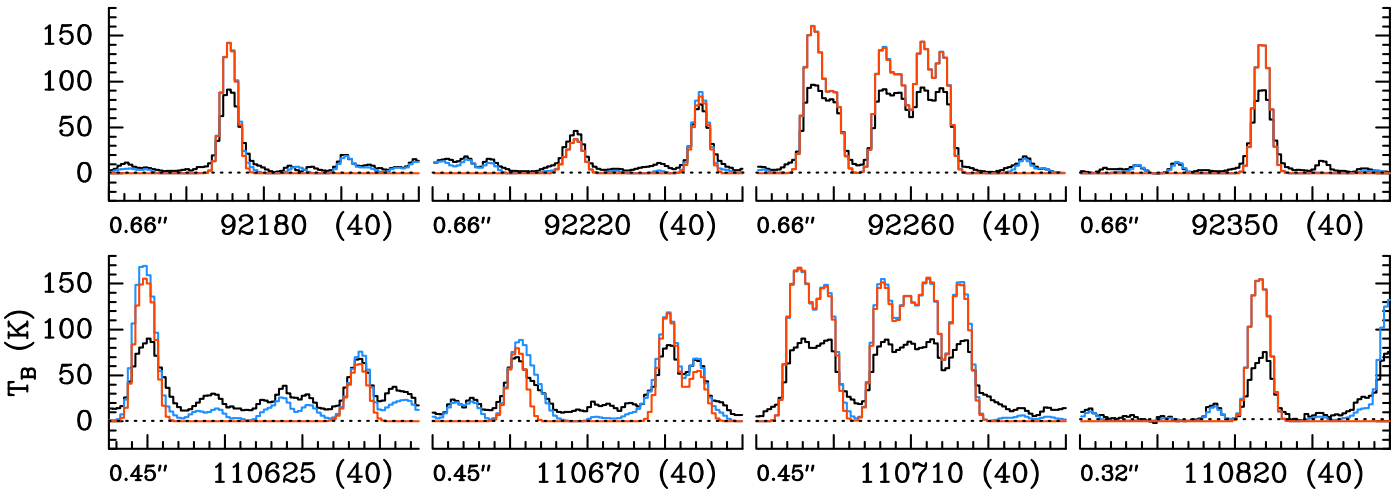

Figure B.13: Same as Fig. B.12 but for CH_3CN, $v_8 = 1$.

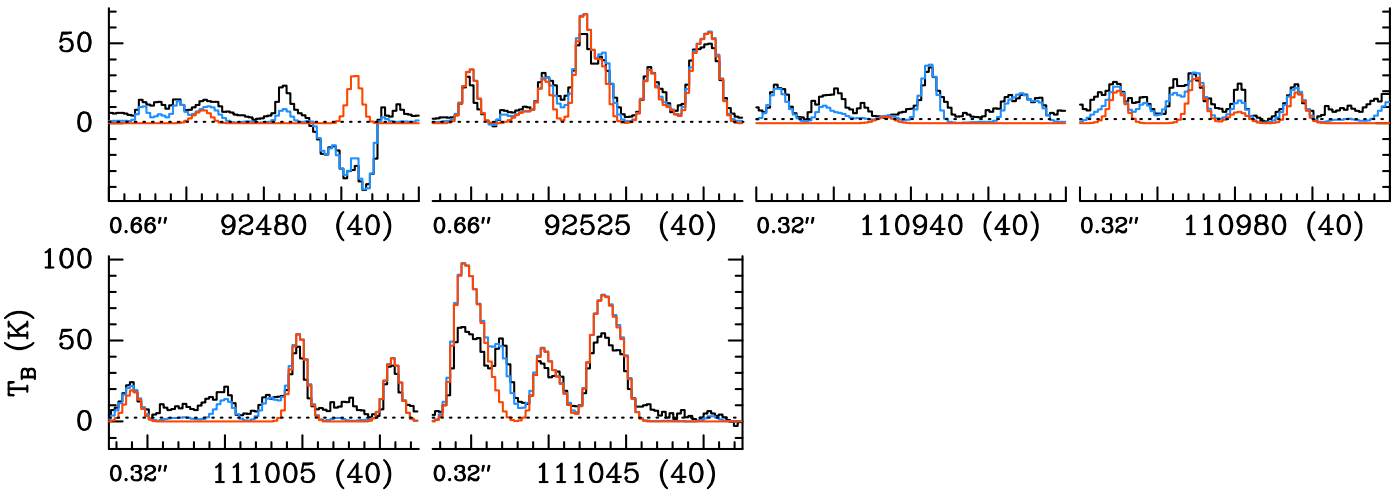

Figure B.14: Same as Fig. B.12 but for CH_3CN, $v_8 = 2$.

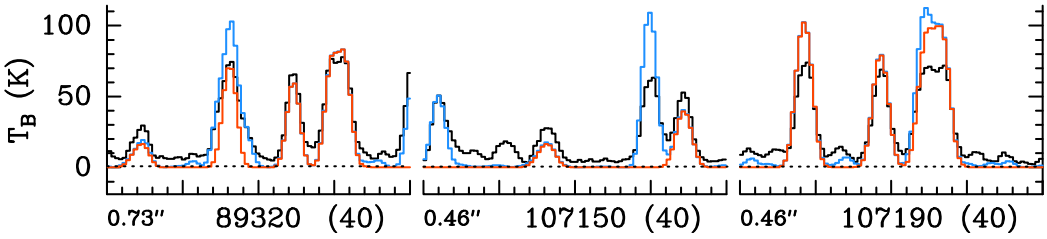

Figure B.15: Same as Fig. B.12 but for $^{13}CH_3CN$, $v = 0$.

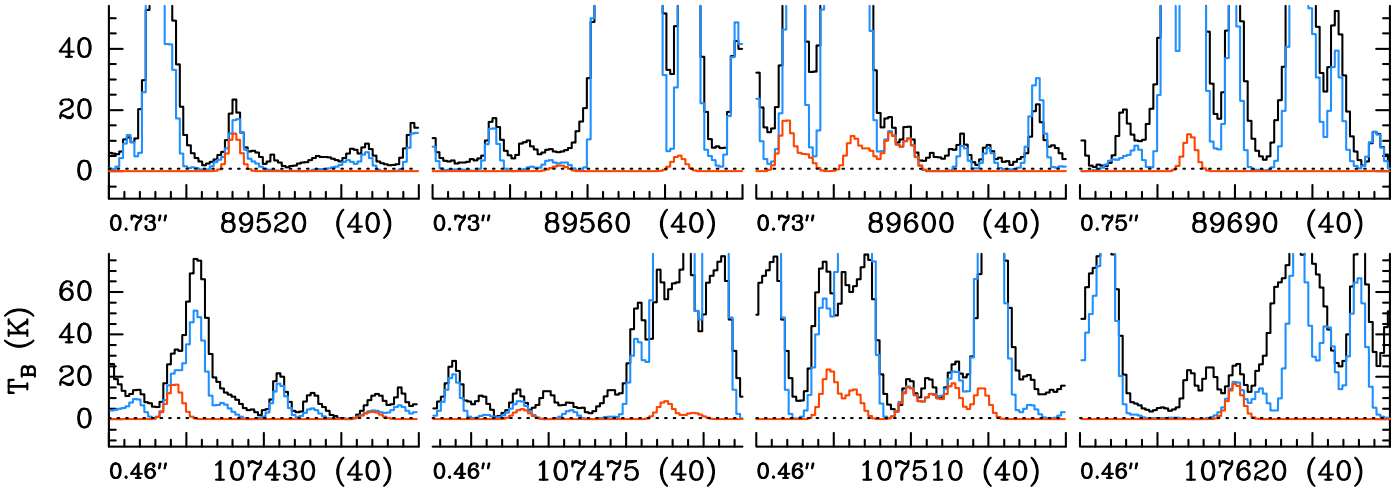

Figure B.16: Same as Fig. B.12 but for $^{13}CH_3CN$, $v_8 = 1$.

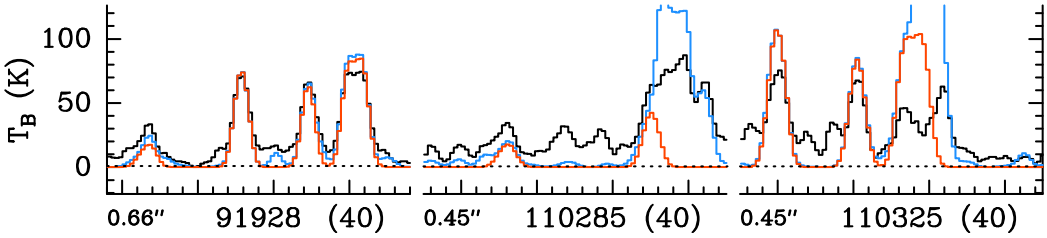

Figure B.17: Same as Fig. B.12 but for $CH_3{}^{13}CN$, $v = 0$.

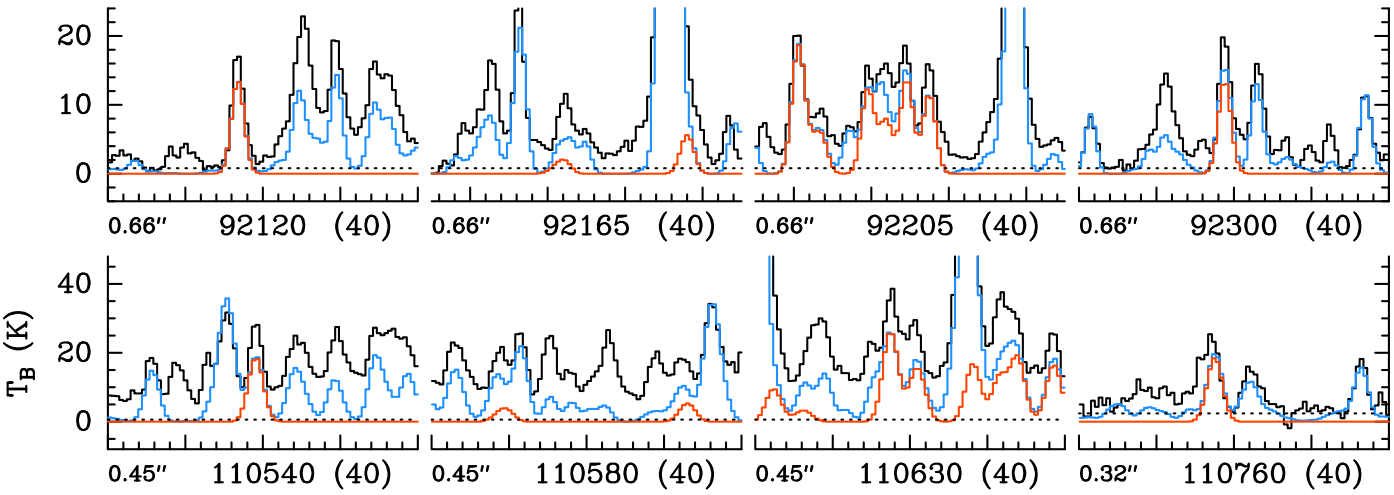

Figure B.18: Same as Fig. B.12 but for $CH_3{}^{13}CN$, $v_8 = 1$.

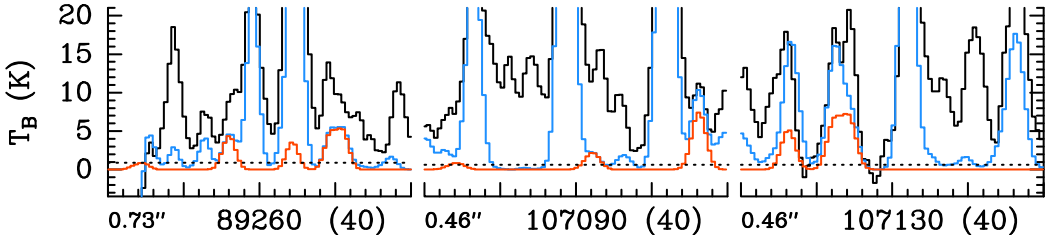

Figure B.19: Same as Fig. B.12 but for $^{13}CH_3{}^{13}CN$, $v = 0$.

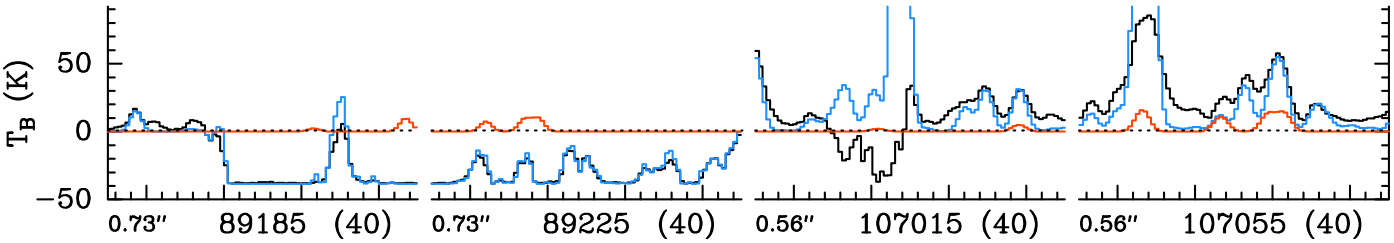

Figure B.20: Same as Fig. B.12 but for $CH_3C^{15}N$, $v = 0$.

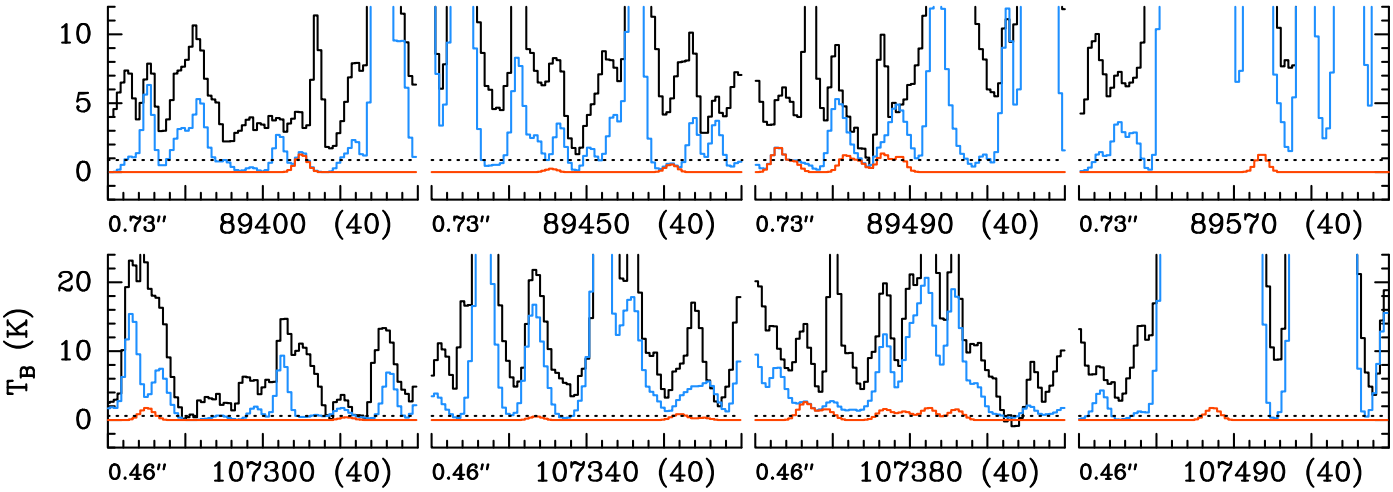

Figure B.21: Same as Fig. B.12 but for $CH_3C^{15}N$, $v_8 = 1$.

Vol. 65, 2010, p. RC12.
URL https://kb.osu.edu/handle/1811/45982

[30] R. Anttila, V. M. Horneman, M. Koivusaari, R. Paso, Ground State Constants A_0, D_0^K and H_0^K of CH_3CN, J. Mol. Spectrosc. 157 (1) (1993) 198–207. doi:10.1006/jmsp.1993.1016.

[31] A. Belloche, R. T. Garrod, H. S. P. Müller, K. M. Menten, I. Medvedev, J. Thomas, Z. Kisiel, Re-exploring Molecular Complexity with ALMA (ReMoCA): interstellar detection of urea, Astron. Astrophys. 628 (2019) A10. arXiv:1906.04614, doi:10.1051/0004-6361/201935428.

[32] G. Winnewisser, A. F. Krupnov, M. Y. Tretyakov, M. Liedtke, F. Lewen, A. H. Saleck, R. Schieder, A. P. Shkaev, S. V. Volokhov, Precision broadband Spectroscopy in the Terahertz Region, J. Mol. Spectrosc. 165 (1) (1994) 294–300. doi:10.1006/jmsp.1994.1132.

[33] M. H. Ordu, H. S. P. Müller, A. Walters, M. Nuñez, F. Lewen, A. Belloche, K. M. Menten, S. Schlemmer, The quest for complex molecules in space: laboratory spectroscopy of n-butyl cyanide, n-C_4H_9CN, in the millimeter wave region and its astronomical search in Sagittarius B2(N), Astron. Astrophys. 541 (2012) A121. arXiv:1204.2686, doi:10.1051/0004-6361/201118738.

[34] M. A. Martin-Drumel, J. van Wijngaarden, O. Zingsheim, F. Lewen, M. E. Harding, S. Schlemmer, S. Thorwirth, Millimeter- and submillimeter-wave spectroscopy of disulfur dioxide, OSSO, J. Mol. Spectrosc. 307 (2015) 33–39. doi:10.1016/j.jms.2014.11.007.

[35] H. S. P. Müller, O. Zingsheim, N. Wehres, J.-U. Grabow, F. Lewen, S. Schlemmer, Rotational Spectroscopy of the Lowest Energy Conformer of 2-Cyanobutane, J. Phys. Chem. A 121 (38) (2017) 7121–7129. doi:10.1021/acs.jpca.7b06072.

[36] L.-H. Xu, R. M. Lees, G. T. Crabbe, J. A. Myshrall, H. S. P. Müller, C. P. Endres, O. Baum, F. Lewen, S. Schlemmer, K. M. Menten, B. E. Billinghurst, Terahertz and far-infrared synchrotron spectroscopy and global modeling of methyl mercaptan, $CH_3{}^{32}SH$, J. Chem. Phys. 137 (10) (2012) 104313. doi:10.1063/1.4745792.

[37] H. S. P. Müller, A. Maeda, S. Thorwirth, F. Lewen, S. Schlemmer, I. R. Medvedev, M. Winnewisser, F. C. De Lucia, E. Herbst, Laboratory spectroscopic study of isotopic thioformaldehyde, H_2CS, and determination of its equilibrium structure, Astron. Astrophys. 621 (2019) A143. arXiv:1812.01554, doi:10.1051/0004-6361/201834517.

[38] B. J. Drouin, F. W. Maiwald, J. C. Pearson, Application of cascaded frequency multiplication to molecular spectroscopy, Rev. Sci. Instr. 76 (9) (2005) 093113. doi:10.1063/1.2042687.

[39] A. G. Maki, J. S. Wells, New Wavenumber Calibration Tables From Heterodyne Frequency Measurements, J. Res. Nat. Inst. Stand. Tech. 97 (4) (1992) 409–470. doi:10.6028/jres.097.019.

[40] L. R. Brown, J. S. Margolis, R. H. Norton, B. D. Stedry, Computer measurement of line strengths with application to the methane spectrum, Appl. Spectrosc. 37 (3) (1983) 287–291. doi:10.1366/0003702834634514.

[41] H. M. Pickett, The fitting and prediction of vibration-rotation spectra with spin interactions, J. Mol. Spectrosc. 148 (2) (1991) 371–377. doi:10.1016/0022-2852(91)90393-0.

[42] B. J. Drouin, H. S. P. Müller, Special issue dedicated to the pioneering work of Drs. Edward A. Cohen and Herbert M. Pickett on spectroscopy relevant to the Earth's atmosphere and astrophysics, J. Mol. Spectrosc. 251 (1-2) (2008) 1–3. doi:10.1016/j.jms.2008.05.004.

[43] J. C. Pearson, H. S. P. Müller, H. M. Pickett, E. A. Cohen, B. J. Drouin, Introduction to submillimeter, millimeter and microwave spectral line catalog, J. Quant. Spectrosc. Radiat. Transfer 111 (2010) 1614–1616. doi:10.1016/j.jqsrt.2010.02.002.

[44] S. E. Novick, A beginner's guide to Pickett's SPCAT/SPFIT, J. Mol. Spectrosc. 329 (2016) 1–7. doi:10.1016/j.jms.2016.08.015.

[45] B. J. Drouin, Practical uses of SPFIT, J. Mol. Spectrosc. 340 (2017) 1–15. doi:10.1016/j.jms.2017.07.009.

[46] H. S. P. Müller, F. Schlöder, J. Stutzki, G. Winnewisser, The Cologne Database for Molecular Spectroscopy, CDMS: a useful tool for astronomers and spectroscopists, J. Mol. Struct. 742 (1-3) (2005) 215–227. doi:10.1016/j.molstruc.2005.01.027.

[47] C. P. Endres, S. Schlemmer, P. Schilke, J. Stutzki, H. S. P. Müller, The Cologne Database for Molecular Spectroscopy, CDMS, in the Virtual Atomic and Molecular Data Centre, VAMDC, J. Mol. Spectrosc. 327 (2016) 95–104. arXiv:1603.03264, doi:10.1016/j.jms.2016.03.005.

[48] J. Gadhi, A. Lahrouni, J. Legrand, J. Demaison, Dipole moment of CH_3CN, J. Chim. Phys. Phys.-Chim. Biol. 92 (1995) 1984–1992. doi:10.1051/jcp/1995921984.

[49] C. P. Rinsland, S. W. Sharpe, R. L. Sams, Temperature-dependent infrared absorption cross sections of methyl cyanide (acetonitrile), J. Quant. Spectrosc. Radiat. Transfer 96 (2) (2005) 271–280. doi:10.1016/j.jqsrt.2005.03.004.

[50] M. Nishio, P. Paillous, M. Khlifi, P. Bruston, F. Raulin, Infrared spectra of gaseous ethanenitrile in the 3500–250 cm^{-1} region: absolute band intensity and implications for the atmosphere of Titan., Spectrochim. Acta 51A (4) (1995) 617–622.

[51] F. Cerceau, F. Raulin, R. Courtin, D. Gautier, Infrared spectra of gaseous mononitriles: Application to the atmosphere of Titan, Icarus 62 (2) (1985) 207–220. doi:10.1016/0019-1035(85)90118-6.

[52] Y. Koga, S. Kondo, S. Saeki, W. B. Person, Infrared intensities of acetonitrile, J. Phys. Chem. 88 (14) (1984) 3152–3157. doi:10.1021/j150658a048.

[53] A. Bauer, S. Maes, Results concerning the rotational spectrum of acetonitrile in the $v_8 = 2$ excited state, C. R. Acad. Sci., Ser. B 268 (1969) 1569.

[54] M. Koivusaari, A. M. Tolonen, R. Paso, J. Schroderus, R. Anttila, The $2\nu_8$ Band of CH_3CN, J. Mol. Spectrosc. 160 (2) (1993) 566–573. doi:10.1006/jmsp.1993.1202.

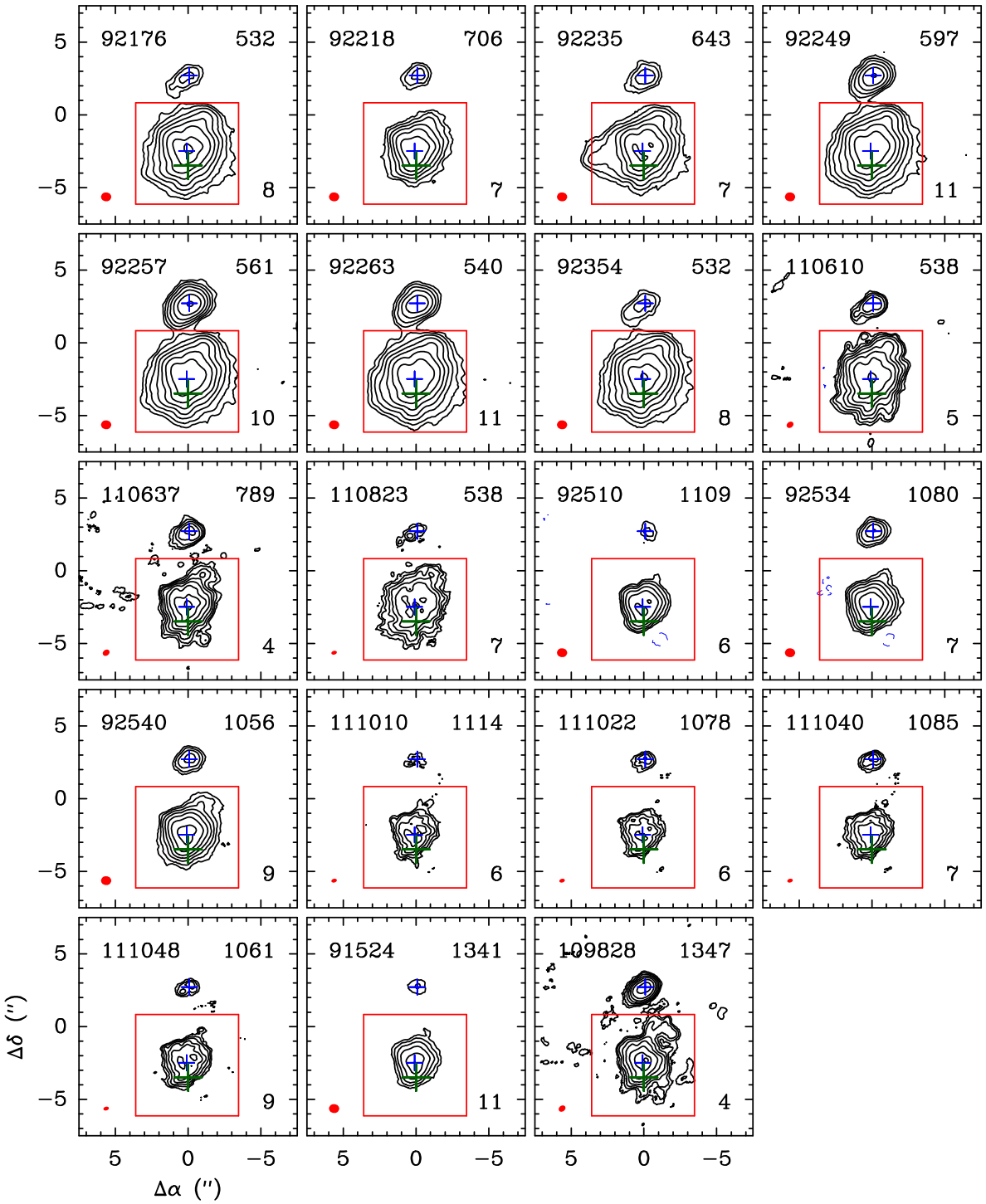

Figure B.22: Integrated intensity maps of transitions or groups of transitions of CH_3CN that are relatively free of contamination from emission of other molecules. From top left to bottom right, the first ten panels show lines from within $v_8 = 1$, the next seven panels lines from within $v_8 = 2$, and the last two panels lines from within $v_4 = 1$. In each panel, the line frequency in MHz is written in the top left corner, the energy of the upper level in K is given in the top right corner, the rms noise level σ in mJy beam^{-1} km s^{-1} is written in the bottom right corner, and the beam (HPBW) is shown in the bottom left corner as a red filled ellipse. The black contour levels start at 6σ and then increase geometrically by a factor of two at each step. The blue, dashed contours show the -6σ level. The bottom and top blue crosses indicate the positions of the hot molecular cores Sgr B2(N1) and Sgr B2(N2), respectively. The green cross marks the position Sgr B2(N1S). Because of the variation in systemic velocity across the field, the assignment of the detected emission to each line is valid only for the region around Sgr B2(N1), highlighted with the red box.

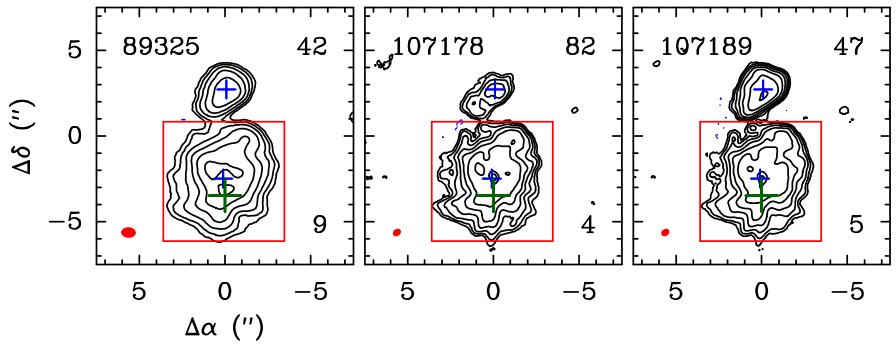

Figure B.23: Same as Fig. B.22 but for $^{13}CH_3CN$ $v = 0$.

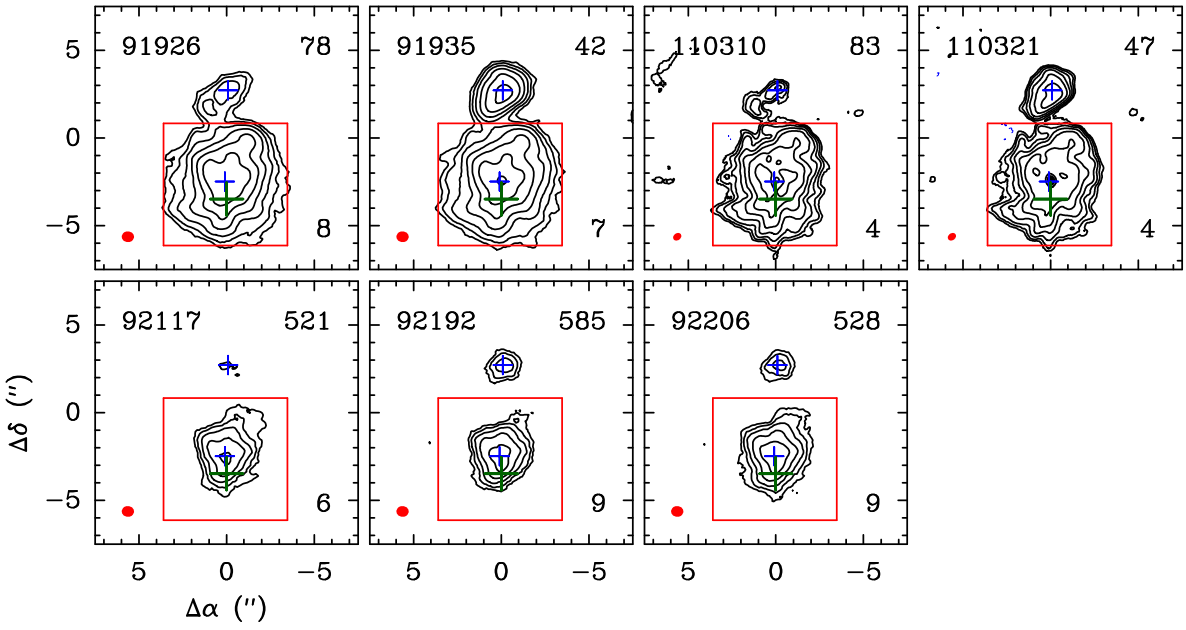

Figure B.24: Same as Fig. B.22 but for $CH_3{}^{13}CN$ $v = 0$ (top row) and $v_8 = 1$ (bottom row).

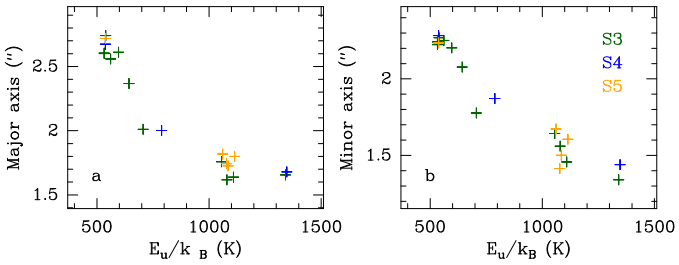

Figure B.25: Deconvolved emission size of uncontaminated CH_3CN transitions as a function of upper-level energy. The major and minor axes (FWHM) are shown in panels a and b, respectively. The observational spectral setups with which the transitions were measured are color-coded as indicated in panel b.

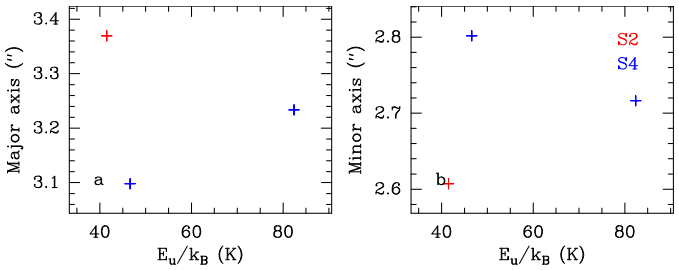

Figure B.26: Same as Fig. B.25 but for $^{13}CH_3CN$.

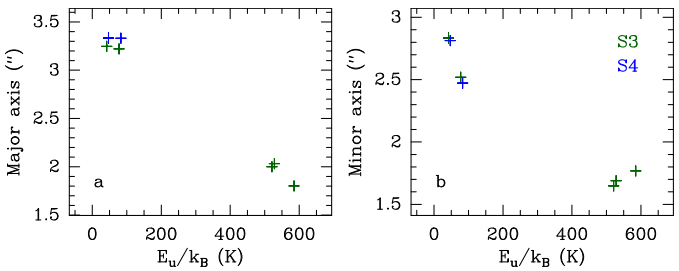

Figure B.27: Same as Fig. B.25 but for $CH_3{}^{13}CN$.

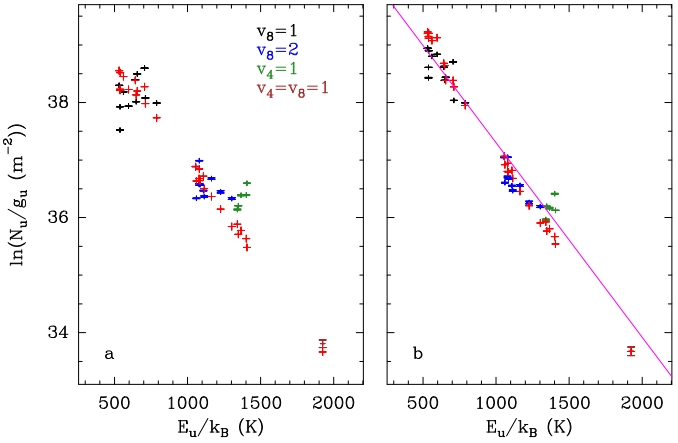

Figure B.28: Population diagram of CH_3CN toward Sgr B2(N1S). The observed datapoints are shown in various colors (but not red) as indicated in the upper right corner of panel a while the synthetic populations are shown in red. No correction is applied in panel a. In panel b, the optical depth correction has been applied to both the observed and synthetic populations and the contamination by all other species included in the full model has been removed from the observed datapoints. The purple line is a linear fit to the observed populations (in linear-logarithmic space).

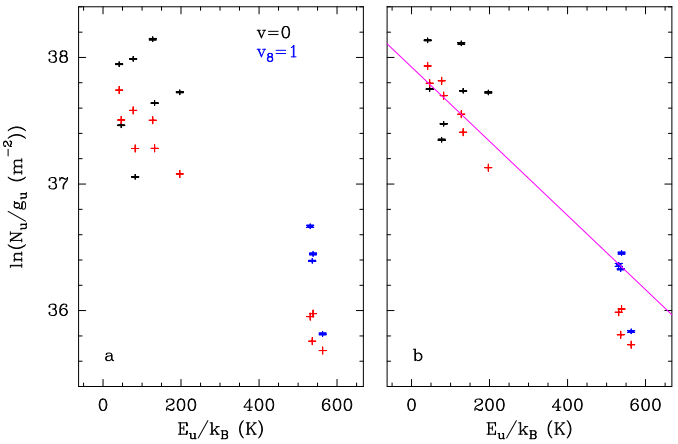

Figure B.29: Same as Fig. B.28 but for $^{13}CH_3CN$.

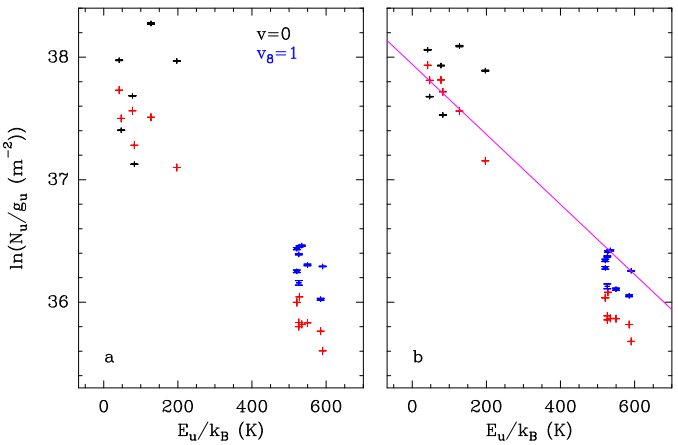

Figure B.30: Same as Fig. B.28 but for $CH_3{}^{13}CN$.

[55] A. Bauer, S. Maes, Millimeter waves of 14-N methyl cyanide and 15-N methyl cyanide. Effects of vibration-rotation interaction and quadrupolar perturbation, J. Phys. (Paris) 240 (1969) 169–180. doi:10.1051/jphys:01969003002-3016900.

[56] W. J. Lafferty, Direct *l*-type doubling transitions in some axially symmetric molecules, J. Mol. Spectrosc. 25 (3) (1968) 359–364. doi:10.1016/S0022-2852(68)80048-7.

[57] J. Cosleou, J. C. López, J. L. Alonso, G. Wlodarczak, J. Demaison, The rotational spectrum of methyl cyanide-D_3. Analysis of the low-lying excited vibrational states, J. Mol. Spectrosc. 149 (1) (1991) 242–251. doi:10.1016/0022-2852(91)90156-5.

[58] M. Koivusaari, V.-M. Horneman, R. Anttila, High-resolution study of the infrared band ν_8 of CH_3CN, J. Mol. Spectrosc. 152 (2) (1992) 377–388. doi:10.1016/0022-2852(92)90076-Z.

[59] G. Cazzoli, C. Puzzarini, The Lamb-dip spectrum of methylcyanide: Precise rotational transition frequencies and improved ground-state rotational parameters, J. Mol. Spectrosc. 240 (2) (2006) 153–163. doi:10.1016/j.jms.2006.09.013.

[60] M. Šimečková, Š. Urban, U. Fuchs, F. Lewen, G. Winnewisser, I. Morino, K. M. T. Yamada, Ground state spectrum of methylcyanide, J. Mol. Spectrosc. 226 (2) (2004) 123–136. doi:10.1016/j.jms.2004.03.013.

[61] S. G. Kukolich, D. J. Ruben, J. H. S. Wang, J. R. Williams, High resolution measurements of ^{14}N, D quadrupole coupling in CH_3CN and CD_3CN, J. Chem. Phys. 58 (8) (1973) 3155–3159. doi:10.1063/1.1679636.

[62] S. G. Kukolich, Beam maser spectroscopy on $J = 1 \rightarrow 2$, $K = 1$, and $K = 0$ transitions in CH_3CN and $CH_3{}^{13}CN$, J. Chem. Phys. 76 (1) (1982) 97–101. doi:10.1063/1.442694.

[63] D. Boucher, J. Burie, J. Demaison, A. Dubrulle, J. Legrand, B. Segard, High-resolution rotational spectrum of methyl cyanide, J. Mol. Spectrosc. 64 (2) (1977) 290–294. doi:10.1016/0022-2852(77)90267-3.

[64] M. J. Reid, K. M. Menten, A. Brunthaler, X. W. Zheng, T. M. Dame, Y. Xu, J. Li, N. Sakai, Y. Wu, K. Immer, B. Zhang, A. Sanna, L. Moscadelli, K. L. J. Rygl, A. Bartkiewicz, B. Hu, L. H. Quiroga-Nuñez, H. J. van Langevelde, Trigonometric Parallaxes of High-mass Star-forming Regions: Our View of the Milky Way, Astrophys. J. 885 (2) (2019) 131. arXiv:1910.03357, doi:10.3847/1538-4357/ab4a11.

[65] M. Melosso, A. Belloche, M. A. Martin-Drumel, O. Pirali, F. Tamassia, L. Bizzocchi, R. T. Garrod, H. S. P. Müller, K. M. Menten, L. Dore, C. Puzzarini, Far-infrared laboratory spectroscopy of aminoacetonitrile and first interstellar detection of its vibrationally excited transitions, Astron. Astrophys. 641 (2020) A160. arXiv:2006.13753, doi:10.1051/0004-6361/202038466.

[66] M. Bonfand, A. Belloche, R. T. Garrod, K. M. Menten, E. Willis, G. Stéphan, H. S. P. Müller, The complex chemistry of hot cores in Sgr B2(N): influence of cosmic-ray ionization and thermal history, Astron. Astrophys. 628 (2019) A27. arXiv:1906.04695, doi:10.1051/0004-6361/201935523.

[67] S. Maret, P. Hily-Blant, J. Pety, S. Bardeau, E. Reynier, Weeds: a CLASS extension for the analysis of millimeter and sub-millimeter spectral surveys, Astron. Astrophys. 526 (2011) A47. arXiv:1012.1747, doi:10.1051/0004-6361/201015487.

[68] J. Demaison, A. Dubrulle, D. Boucher, J. Burie, V. Typke, Microwave spectra, centrifugal distortion constants, and r_z structure of acetonitrile and its isotopic species, J. Mol. Spectrosc. 76 (1-3) (1979) 1–16. doi:10.1016/0022-2852(79)90214-5.

[69] A. Bauer, G. Tarrago, A. Remy, Analysis of the rotational spectrum of C_{3v} molecules by using factorization and diagonalization of the energy matrix. Application to $CH_3C^{15}N$, J. Mol. Spectrosc. 58 (1) (1975) 111–124. doi:10.1016/0022-2852(75)90160-5.

[70] R. A. Motiyenko, A. Belloche, R. T. Garrod, L. Margulès, H. S. P. Müller, K. M. Menten, J. C. Guillemin, Millimeter- and submillimeter-wave spectroscopy of thioformamide and interstellar search toward Sgr B2(N), Astron. Astrophys. 642 (2020) A29. arXiv:2009.07592, doi:10.1051/0004-6361/202038723.

[71] H. S. P. Müller, A. Belloche, K. M. Menten, C. Comito, P. Schilke, Rotational spectroscopy of isotopic vinyl cyanide, H_2CCHCN, in the laboratory and in space, J. Mol. Spectrosc. 251 (1-2) (2008) 319–325. arXiv:0806.2098, doi:10.1016/j.jms.2008.03.016.

[72] H. S. P. Müller, A. Belloche, L.-H. Xu, R. M. Lees, R. T. Garrod, A. Walters, J. van Wijngaarden, F. Lewen, S. Schlemmer, K. M. Menten, Exploring molecular complexity with ALMA (EMoCA): Alkanethiols and alkanols in Sagittarius B2(N2), Astron. Astrophys. 587 (2016) A92. arXiv:1512.05301, doi:10.1051/0004-6361/201527470.

[73] D. Begue, P. Carbonniere, C. Pouchan, Calculations of Vibrational Energy Levels by Using a Hybrid ab Initio and DFT Quartic Force Field: Application to Acetonitrile, J. Phys. Chem. A 109 (20) (2005) 4611–4616. doi:10.1021/jp0406114.

[74] G. Avila, T. Carrington, Using nonproduct quadrature grids to solve the vibrational Schrödinger equation in 12D, J. Chem. Phys. 134 (5) (2011) 054126. doi:10.1063/1.3549817.

[75] T. Halverson, B. Poirier, Large scale exact quantum dynamics calculations: Ten thousand quantum states of acetonitrile, Chem. Phys. Lett. 624 (2015) 37–42. doi:10.1016/j.cplett.2015.02.004.